Pergamon

PII: S0191-8141(98)00038-8

Journal of Structural Geology, Vol. 20, No. 8, pp. 1043 to 1063, 1998

0191-8141/98 $19.00 + 0.00

Late Miocene to Recent transtensional tectonics in the Sierra San Fermín, northeastern Baja California, Mexico

CLAUDIA J. LEWIS*

Department of Earth and Planetary Sciences, Harvard University, 24 Oxford Street, Cambridge, MA 02138, U.S.A. E-mail: clewis@lanl.gov

and

JOANN M. STOCK

Seismological Laboratory 252-21, California Institute of Technology, Pasadena, CA 91125, U.S.A.

(*Received* 4 *March* 1997; *accepted in revised form* 31 *March* 1998)

Abstract—Basins and ranges within part of the Gulf of California Extensional Province (Mexico) have experienced complex distributed deformation, including normal and strike-slip faulting and block rotations, linked to dextral shear at the Pacific–North America plate boundary. In the Sierra San Fermín and southern Sierra San Felipe (northeastern Baja California), normal faulting began between 12.5 and 6 Ma, although most extension occurred between about 6 and 3 Ma, strongly influencing thickness and distribution of ash-flow tuffs and sedimentary deposits. Extension is generally $< 10\%$ in 6 Ma rocks and somewhat more in 12.5 Ma rocks. Inversion of kinematic data, interpreted together with published paleomagnetic data, suggests that the axis of least principal stress was oriented between W–E and SW–NE in late Miocene time. Our data indicate an important change in the amount of dextral shear, but not necessarily the least principal stress direction (WSW–ENE), at about 3 Ma. Structural constraints limit significant sinistral strike-slip faulting, conjugate to the dextral plate boundary, to the last ~3 My. Progressive changes in the geometry of faulting through time are consistent with regional strain partitioning within the Pacific–North America plate boundary zone, and are predicted by physical and analytical models of oblique divergence as the orientation of the stretching vector α changes to lower and lower values.

STRUCTURAL EVOLUTION OF THE GULF OF CALIFORNIA

The Pacific–North America plate boundary in southern California and western Mexico is a complex array of late Cenozoic oceanic transform faults and spreading ridges, continental dextral and sinistral strike-slip faults, and associated normal and reverse faults that has deformed the western margin of North America and transferred a continental sliver, the Baja California Peninsula, to the Pacific plate (Fig. 1). Growing geological interest in the origin of continental rifting within the Gulf of California, and its development into an integrated system of spreading ridges and transform faults, stems from the realization that oceanic crust in the mouth of the Gulf does not record the entire history of rifting in this area (e.g. Moore and Buffington, 1968; Mammerickx and Klitgord, 1982; Curray and Moore, 1984).

When transform motion was initiated in the Gulf is not known directly, but it has long been thought that seafloor spreading began when the modern San Andreas fault became active about 5.5 Ma. However, the oldest oceanic crust in the mouth of the Gulf unequivocally associated with Pacific–North America spreading is 3.4 Ma in age, recording 175 km of seafloor spreading between the Pacific and North American plates (Larson *et al.*, 1968; Mammerickx and Klitgord, 1982; DeMets *et al.*, 1987; Lonsdale, 1989). Additional transform motion, required to total 300 km of displacement on Gulf transform faults suggested by geologic constraints (Gastil *et al.*, 1973, 1981), is thought to have occurred between 5.5 and 3.4 Ma (Curray and Moore, 1984; Lonsdale, 1989). Nevertheless, abundant geological evidence of late Miocene extension and subsidence in the Gulf region (e.g. Dokka and Merriam, 1982; Stock and Hodges, 1989, 1990; Lee *et al.*, 1996) indicates that the Pliocene phase of rifting, related to dextral slip between the Pacific and North American plates, was preceded by a 'proto-Gulf' phase (e.g. Karig and Jensky, 1972).

It is generally accepted that late Oligocene to middle Miocene arc volcanism and/or middle to late Miocene extension weakened the crust in the vicinity of the modern Gulf, facilitating propagation of the Pacific–North America plate boundary into the Gulf in Pliocene time (Gastil, 1968; Dokka and Merriam, 1982; Curray and Moore, 1984; Henry, 1989). The tectonic setting of circum-Gulf extension is controversial, however. Late Cenozoic normal faulting in the Gulf Region has been related by some investigators to dis-

*Now at: Los Alamos National Laboratory, EES-1, MS D462, Los Alamos, NM 87545.

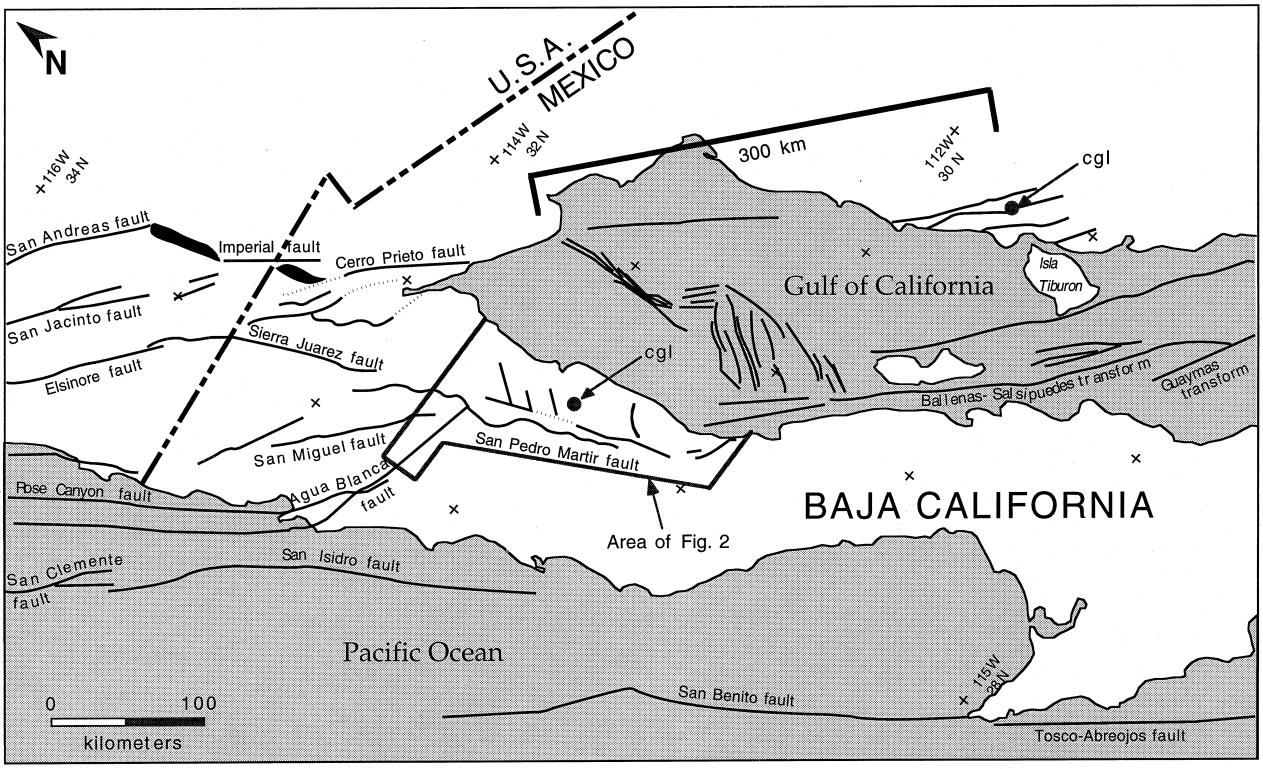

Fig. 1. Map of southern California, Baja California, and the western Mexican mainland showing principal structures in the broad, deforming zone between the Pacific and North American plates (after Goddard *et al.*, 1965; Gastil and Krummenacher, 1977; Fenby and Gastil, 1991; Lyle and Ness, 1991). Dash–dot line represents international border. Filled circles labeled 'cgl' indicate outcrops of distinctive conglomerate used as piercing point for determination of 300 km dextral slip across Gulf transform faults (Gastil *et al.*, 1973).

tension of the Basin and Range Province of southwestern North America (Dokka and Merriam, 1982; Henry, 1989). Others directly relate middle to late Miocene extension to the development of the Pacific–North America plate boundary (e.g. Gastil and Krummenacher, 1977; Spencer and Normark, 1979; Hausback, 1984). Extension in the Gulf region, and changes in the rates and directions of extension, may have occurred as a result of strain partitioning between strike-slip faults in the Pacific margin and normal faults in the Gulf Extensional Province in accordance with changes in the direction of Pacific–North America relative motion. Recent plate reconstructions are consistent with geological constraints which demonstrate (1) the slow transfer of Baja California from the North American to the Pacific plate, beginning well before 6 Ma; (2) the association of normal and strike-slip faulting in the plate boundary; and (3) changes in the rate and direction of extension as the modern plate boundary became well-established in the Gulf (Stock and Hodges, 1989).

The amount and direction of extension and shear are strong constraints on models of the structural evolution of the Gulf region. Detailed kinematic analyses of late Miocene to Recent faulting are therefore indispensable to a better understanding of the processes that brought about continental rifting along this portion of the plate boundary. Our work in the northern Puertecitos Volcanic Province (Fig. 2) indicates that normal faulting characterized the structural style in late Miocene time, but that this style changed in late Pliocene time to combined normal and sinistral faulting as the direction of relative Pacific–North America plate motion became less oblique and the Gulf became the principal locus of relative plate motion.

GEOLOGIC SETTING OF THE GULF EXTENSIONAL PROVINCE, NORTHEASTERN BAJA CALIFORNIA

The Sierra San Fermín and Sierra San Felipe (between latitudes 30° 30′ and 30° 44′N and longitudes 114° 42′ and 114° 51′W), in northeastern Baja California, Mexico, are located within the Gulf Extensional Province, a region of late Miocene to Recent volcanism, crustal extension and dextral shear at the Pacific–North America plate boundary (Figs 1 & 2). The study area comprises part of the late Oligocene to middle Miocene, subduction-related volcanic arc which extended the length of the Baja California peninsula, and the middle Miocene to Recent, extension-related Puertecitos Volcanic Province (Fig. 2). The region straddles two major vents of 12.5 and ~6 Ma in age, sources for regionally

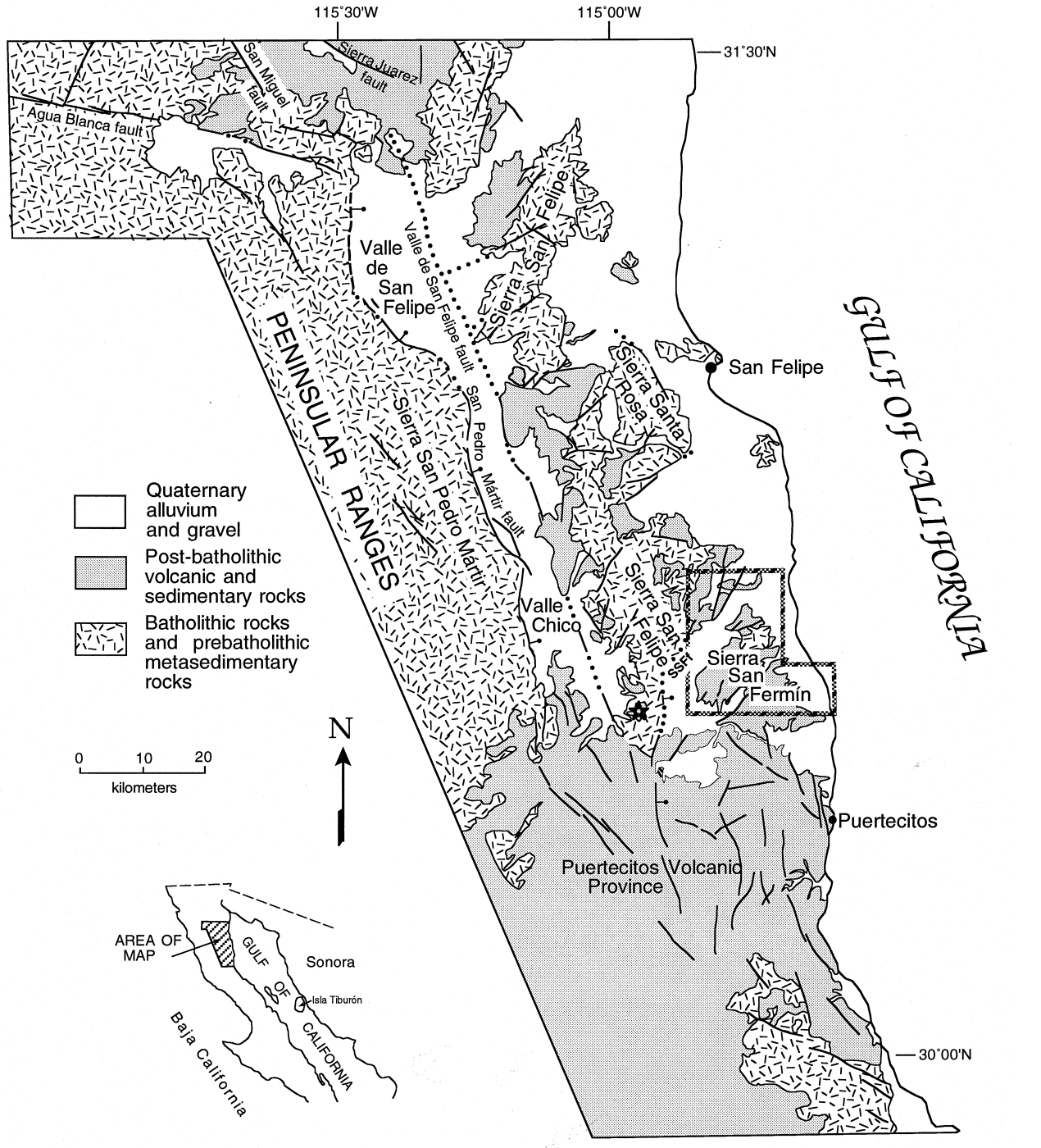

Fig. 2. Regional geologic map of northeastern Baja California. SSFf is Sierra San Felipe fault. Area of Fig. 3 indicated by box. Star shows location of Mesa Cuadrada. Modified from Gastil *et al.* (1975).

extensive rhyolitic ash-flow tuffs that were subsequently dismembered by both normal and strike-slip faulting (Lewis, 1996; updated by geochronology of Stock *et al.*, 1997).

The Tertiary stratigraphy of the Sierra San Fermín and the southern Sierra San Felipe is divided into five informal groups based on subtle but important unconformities associated with Neogene extensional and strike-slip faulting (Fig. 3 inset; Lewis, 1996). Group 1 comprises basement-derived arkosic sandstone, basalt and pyroclastic flows, and volcaniclastic sedimentary rocks approximately early to middle Miocene in age. Group 2 consists of up to 200 m of pyroclastic flows, basalt and hornblende andesite flows, and reworked volcanic sedimentary rocks ranging in age from <12.5 to >6 Ma. Group 3 consists of a sequence of pyroclastic flows, ash fall deposits, and rhyolite flows, all $\sim$6 Ma. The tuffs in this sequence thicken toward the south across a structural discontinuity. The youngest of these tuffs appears to have ponded against a WSW–

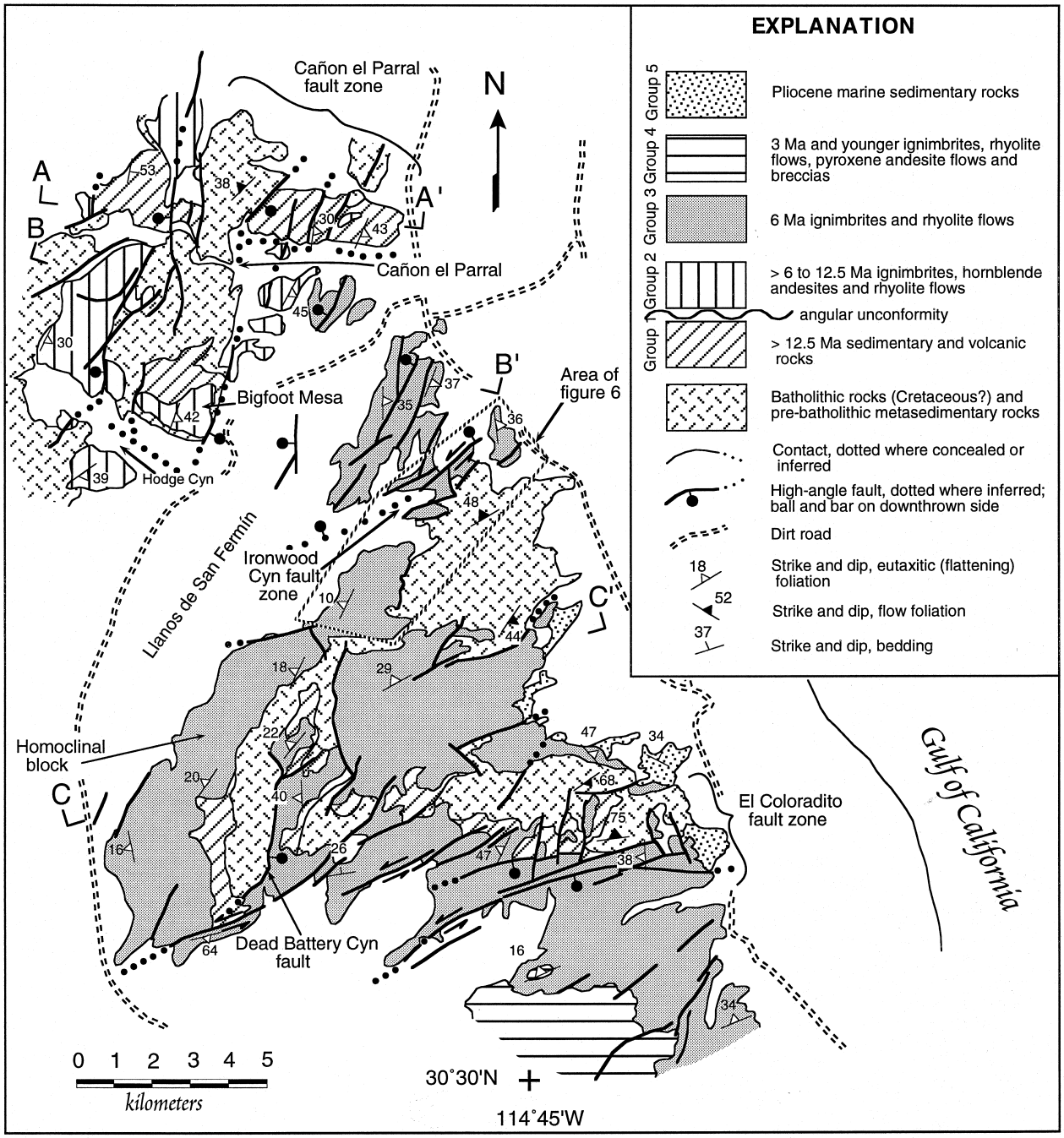

Fig. 3. Generalized geologic map showing principal structures and geographic features of area. See Fig. 2 for location. Area of Fig. 6 indicated by box. Cyn = Canyon.

ENE structural barrier, causing them to be very thin to absent north of this boundary. Group 4 consists of pyroclastic flows and ~300 m of pyroxene andesite flows and breccias, all ~3 Ma in age. Group 5 comprises alluvial and marine sedimentary units deposited in fault-controlled basins in latest Miocene through Pliocene time. These group divisions are similar to, but not exactly the same as, group divisions established in correlative rocks in the southern Valle Chico region to the west (Fig. 2; Stock, 1989, 1993; Stock and Hodges, 1990).

Structural interpretations in the present study area are based on offsets of beds within Groups 2–5, particularly the thin, extensive, welded tuffs useful as stratigraphic markers (the 12.5 Ma Tuff of San Felipe of Group 2; the 6.5 Ma Tmr3b of Group 3; and the 3 Ma Tuffs of Mesa El Tábano of Group 4; Fig. 3 inset). An angular discordance between the Tuff of San Felipe and overlying 6 Ma tuffs indicates the onset of normal faulting in this area (Stock and Hodges, 1990; Lewis, 1996). Although less deformed than the middle to late Miocene ignimbrites, the 3 Ma

Tuffs of Mesa El Tábano are affected by normal and strike-slip faulting, which continues today.

The western boundary of the extensional province at this latitude is the Main Gulf Escarpment, which separates the relatively unextended batholithic rocks of the Peninsular Ranges, on the west, from the lower-elevation basins and ranges of the Gulf Extensional Province to the east (Fig. 2). The E-dipping San Pedro Mártir fault, the principal fault of the escarpment at this latitude, strikes approximately NNW for ~100 km and has up to 5 km of normal separation (Hamilton, 1971; Slyker, 1974). Structural relief began developing at its southern end between 12.5 and 6 Ma (Stock and Hodges 1989; updated by geochronology of Stock *et al*., 1997), and Holocene scarps indicate that the San Pedro Mártir fault is still active (Gastil *et al*., 1975; Brown, 1978). The amount of extension across a 10-km-long transect near the southern end of the fault is ~10%, half of this amount occurring between 12.5 and 6 Ma and half in the last 6 My (Stock, 1993; updated by geochronology of Stock *et al*., 1997).

An accommodation zone in southern Valle Chico (Fig. 2; first hypothesized by Dokka and Merriam, 1982) transfers slip from the San Pedro Mártir fault southeastward onto transform faults in the Gulf of California (Stock and Hodges, 1990). The accommodation zone affects the pattern and geometry of the footwall (escarpment) faults and may indicate differential extension and/or a difference in depth to the basal detachment fault (Stock and Hodges, 1990). An alternative explanation attributes this accommodation zone to a reversal in vergence above major listric fault systems (Axen, 1995).

Two major dextral strike-slip faults, the Agua Blanca fault (striking WNW) and the San Miguel fault (striking NW) transect the Peninsular Ranges but die out eastward as they approach the Main Gulf Escarpment approximately 100 km NW of the study area (Fig. 2). These faults have been interpreted as intracontinental transform faults (transcurrent faults), transferring some of the slip from transform faults in the Gulf across the peninsula into the continental borderland (Hamilton, 1971; Legg *et al*., 1991; Grover *et al*., 1993). However, they do not connect directly along strike into the Gulf of California. Rather, diffuse dextral shear may be accommodated by numerous normal and strike-slip faults both within the Sierra San Pedro Mártir (e.g. Valle Trinidad; Allen *et al*., 1960) and in the basins and ranges to the east (Fig. 2; Lewis and Stock, *in press*). The NNW-striking Valle de San Felipe–Valle Chico, for example, located between the Sierra San Felipe and the Main Gulf Escarpment, may be an oblique pull-apart basin formed by the partitioning of dextral displacement onto the normal San Pedro Mártir fault and oblique normal or dextral Valle de San Felipe fault (Stock and Hodges, 1990; Grover *et al*., 1993).

In the basins and ranges east of the Main Gulf Escarpment, numerous N-striking normal faults and NE-striking sinistral faults bound ranges separated by late Miocene/Pliocene marine and alluvial basins (Hamilton, 1971; Bryant, 1986; Stock, 1993; Lewis, 1994). The Sierra San Fermín and southern Sierra San Felipe are two of the many ranges in this area, and are the focus of this study (Fig. 2). Declinations of characteristic magnetization from a series of middle to late Miocene and Pliocene welded ash-flow tuffs indicate that fault blocks within these ranges have been rotated ~30° clockwise about vertical axes since Miocene time (post-6 Ma; Lewis and Stock, in press). Localized rotation about vertical axes is a significant component of strain in this area, and may result from oblique extension of the hanging wall of the San Pedro Mártir fault associated with dextral displacement between the Pacific and North American plates (Lewis and Stock, in press).

TRANSTENSIONAL GEOMETRY

Geometry and timing of extensional faulting and sinistral shear

The principal faults in the area are N- to NE-striking normal faults, ENE-striking sinistral strike-slip faults, and NE-striking sinistral normal faults (Fig. 4a). The youngest faults in the area, which cut Quaternary strata, have orientations and senses of slip similar to the principal faults (Fig. 4b). Because the orientations of the youngest faults coincide with orientations of the principal faults, the direction of maximum elongation may have remained constant since late Miocene time.

Approximately 120 measurements of striated fault planes were made in the Sierra San Fermín and Sierra San Felipe (Fig. 5). The data exhibit considerable heterogeneity in fault orientation and slip. Clockwise block rotations in this area have caused vertical-axis rotations of fault planes (Lewis and Stock, in press), and therefore undoubtedly contribute to scatter. Because this data set may contain faults of more than one age which have undergone varying degrees of vertical-axis rotation, we have separated the data into two groups (Fig. 5). Group 1 faults include those which cut middle to late Miocene rocks (stratigraphic Groups 1, 2 and 3), and Group 2 faults include those which cut Pliocene rocks (stratigraphic Groups 4 and 5) and Quaternary strata. The Group 1 fault set may, however, contain fault/slickenline data attributable to Pliocene/Quaternary time. Many of the NE- to ENE-striking major faults in the Ironwood Canyon and El Coloradito fault zones (Fig. 3), for example, show sinistral normal or sinistral slickenlines superposed on dip-slip slickenlines, indicating reactivation.

The majority of faults in both groups have a sinistral component (53% of the Group 1 faults, and 67%

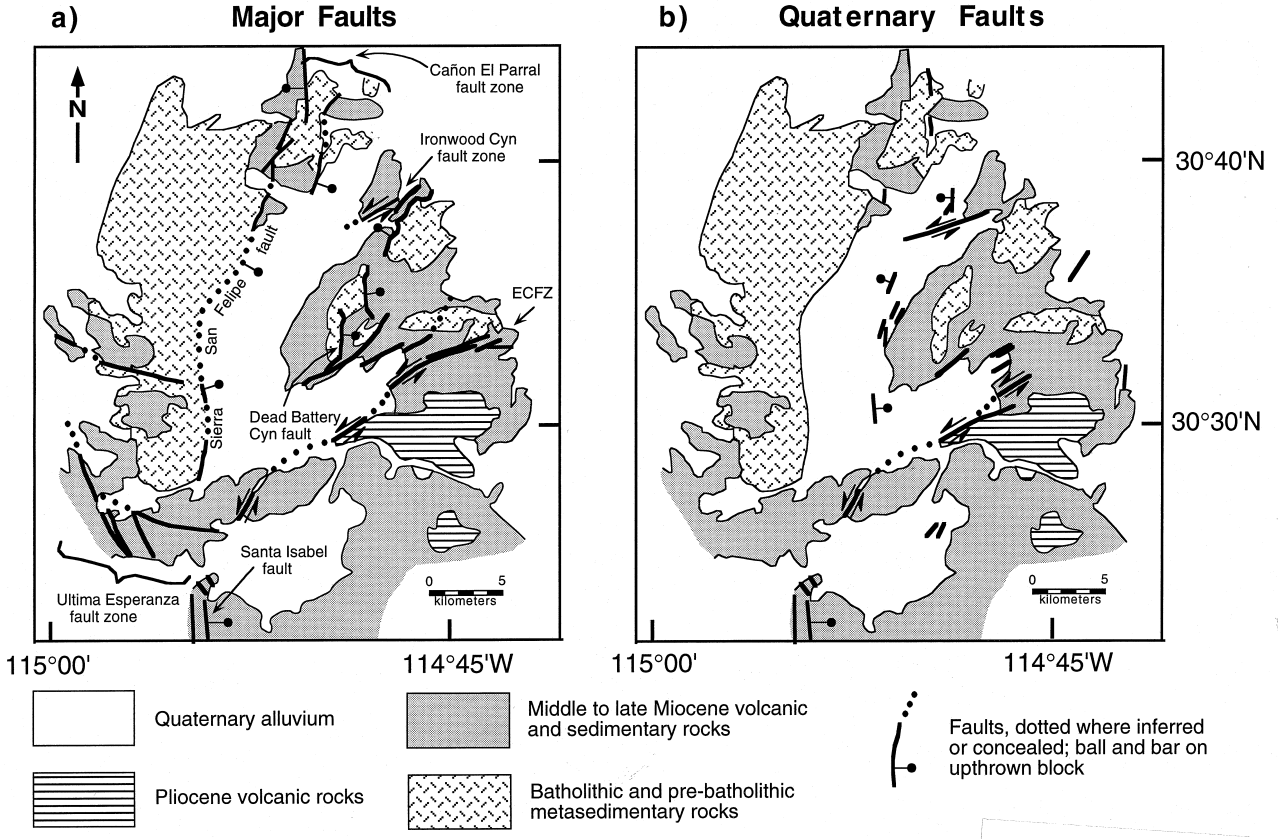

Fig. 4. Fault maps of the Sierra San Fermín and part of the southern Sierra San Felipe: (a) largest faults in the area, and (b) Quaternary fault scarps. Southern quarter from Stock *et al.* (1991) and Stock (1993); otherwise from Lewis (1994).

of the Group 2 faults). Many faults have experienced oblique offset, but there is no clear relationship between dip and rake (Fig. 5). If we say that faults with rakes $\geq 70^\circ$ are dominantly normal, and those with rakes $\leq 20^\circ$ are dominantly strike-slip, then more than a third of the faults in Group 1 are oblique, though nearly as many are dextral (15% of $n = 91$) as sinistral (20% of $n = 91$). It is clear, however, that of the faults with rakes $\leq 20^\circ$, most are sinistral; among Group 1 and Group 2 faults, nearly 80% of these are sinistral. The ubiquitous oblique component of slip suggests that the direction of extension is not perpendicular to the average northerly strike of the principal normal faults. Paleomagnetic evidence for vertical-axis block rotations, and structural evidence for major ENE-striking normal faults reactivated as sinistral faults, therefore call for caution in assigning extension directions based on fault strikes alone.

Sierra San Felipe fault zone. The Sierra San Felipe fault zone is a major structural boundary, 20 km east of the Main Gulf Escarpment, between two principal range blocks, the Sierra San Fermín and the southern Sierra San Felipe (Fig. 2). The latter is capped by a west-tilted mesa at ~1100 m, Mesa Cuadrada (Fig. 2), comprising middle to late Miocene ash-flow tuffs. About 3 km east of Mesa Cuadrada, near the range-front of the Sierra San Felipe, this same section, tilted westward, crops out at elevations of ~400 m. Geologic relations require an east-dipping range-front fault or fault zone to be present beneath alluvium along the eastern edge of the Sierra San Felipe (Fig. 2), though only the eroded escarpment is visible today. Normal separation of the 12.5 Ma Tuff of San Felipe is about 800 m (Stock, 1993). This is similar to the amount of normal separation on the Main Gulf Escarpment fault system in southern Valle Chico to the west, suggesting that the Sierra San Felipe fault zone may be one of the principal structures of the extensional province (Stock and Hodges, 1990).

The eastern escarpment of the Sierra San Felipe formed sometime after 6 Ma (Stock *et al.*, 1991; Stock, 1993; Lewis, 1994). No Quaternary scarps cut the alluvium along the Sierra San Felipe range-front. Pliocene scarps may have been buried by the large volume of sediment derived from the adjacent granitic range. However, along strike to the south, the Sierra San Felipe fault zone splays into a set of faults that are overlain by unfaulted tuffs thought to be late Miocene in age (Stock *et al.*, 1991; Stock, 1993; Nagy, 1997).

The Sierra San Fermín is in large part the hanging wall of the east-dipping Sierra San Felipe fault (Fig. 2). The western part of the Sierra San Fermín is a homoclinal, hanging wall block in which middle to late Miocene tuffs dip 15–20° west towards the range-front

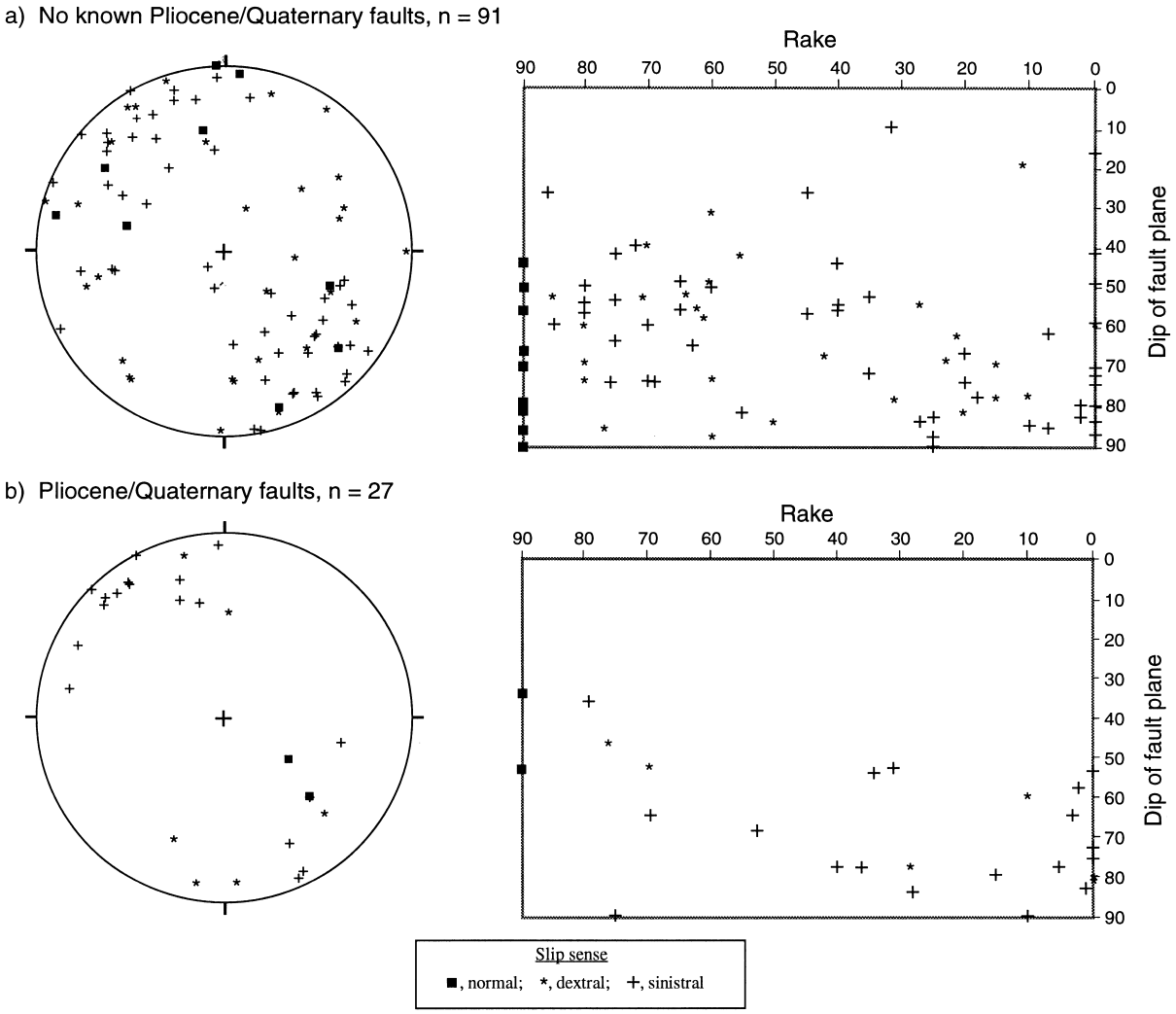

Fig. 5. Equal area projections of (a) poles to Group 1 fault planes, which cut rocks older than Pliocene (N = 91), and (b) poles to Group 2 fault planes, which cut Pliocene/Quaternary rocks (N = 27). Symbols indicate sense of slip determined from kinematic indicators (striae, grooves, or slickenlines) in fault planes and fault separation.

fault of the Sierra San Felipe (Fig. 3). Angular discordance between ash-flow tuffs in the Sierra San Fermín indicates that extension began here between 12.5 and 6 Ma (Lewis, 1996; updated by geochronology of Stock *et al*., 1997). Normal faulting within the hanging wall continued as the dominant style of deformation well into Pliocene time and even occurs today. In the Llanos de San Fermín (Fig. 3), the alluvial plain east of the Sierra San Felipe, mapped N- and NE-striking scarps cut Quaternary alluvium (Dokka and Merriam, 1982; Lewis, 1994).

Ironwood Canyon detachment fault. The NE-striking Ironwood Canyon fault zone (Figs 3 & 6) includes the Ironwood Canyon detachment fault and the Delicias fault zone, an anastamosing array of sinistral faults. The Ironwood Canyon detachment fault projects NW beneath a region of E- to SE-dipping, normal-fault bounded domino blocks, found in the northernmost Sierra San Fermín and the Cañon El Parral area of the Sierra San Felipe (Fig. 3). Faulting along ENE- to NE-striking faults began in this area not long after deposition of the 12.5 Ma Tuff of San Felipe (Group 2) and continued until after deposition of 6 Ma tuffs (Group 3). Domino faulting produced a supradetachment basin which preserves the upper unwelded portions of a 6 Ma tuff (Group 3) and a thick section of latest Miocene/Pliocene lacustrine or marine mudstones grading up into coarse, alluvial conglomerates (Group 5; Lewis, 1994). Further normal faulting tilted bedding in Group 5 strata up to about 40°, although domino faulting does not affect these rocks. Therefore, normal faulting was probably most active here between latest Miocene and late Pliocene time (~6–3 Ma).

Delicias fault zone. The Delicias fault zone, a major ENE-striking (~060°) sinistral fault system in the Ironwood Canyon area, contains many anastamosing, steeply-dipping faults which cut the Ironwood Canyon detachment fault (Fig. 6). ENE-striking faults in this zone have undergone nearly pure sinistral slip, whereas numerous NE-striking faults have sinistral normal slip indicators and may be Riedel shears along the major ENE-striking sinistral faults.

Faults in the Delicias fault zone cut Pliocene sedimentary rocks (Group 5) but do not appear to have controlled depositional patterns in them, suggesting that sinistral-slip faulting began in late Pliocene time. Strike-slip faulting thus began after deposition of Group 5 rocks and continued into Quaternary time (Lewis, 1994). The Delicias fault zone projects southwestward across the Llanod de San Fermín (Fig. 3), where it controls entrenchment patterns in Quaternary alluvium.

Cañon El Parral fault zone. From a single, east-side-down strand west of the Sierra San Fermín homoclinal block (Fig. 2), the Sierra San Felipe fault curves northeastward and passes into the Cañon El Parral fault zone, an 8-km wide zone of dominantly down-to-the-west normal faults (Fig. 3). The 12.5 Ma Tuff of San Felipe in this fault zone is pervasively deformed by closely spaced (about 1 m apart), N- to NNE-striking, moderately to steeply W-dipping (43–73°) normal faults, generally with dip-slip or oblique-slip striae. There are several faults in the Cañon El Parral fault zone with large normal separations (totalling 1 km), but none appear to be longer than about 5 km. Displacement is transferred, both north and south along strike, onto numerous splays of smaller displacement. This pattern of faulting persists southeastward across the northern Sierra San Fermín and ends at the Ironwood Canyon fault. A very few strike-slip slickenlines were observed in the Cañon El Parral fault zone; slickenlines on one NNW-striking fault indicate down-to-the-west dextral normal slip.

The absence of a major, E-dipping normal fault near the range front in the Cañon El Parral area, combined with the systematic tilt of fault blocks toward the Ironwood Canyon fault, suggests that the Cañon El Parral area is the hanging wall of the Ironwood Canyon fault. The change in the geometry of the Sierra San Felipe range-front system, and the reversal in vergence between the Sierra San Felipe and Ironwood Canyon faults, suggest that both the Sierra San Felipe and Sierra San Fermín may ride in the hanging wall of a deeper detachment, perhaps the eastward extension of the San Pedro Mártir fault (Fig. 2). In this case, the vergence reversal constitutes a major break in upper plate structure. Inferred ESE-striking faults in the eastern range-front of the Sierra San Felipe, in Cañon El Parral and the canyon directly south of it, may be tear faults that partially accommodate the vergence reversal (Fig. 3; Lewis, 1994).

El Coloradito fault zone. The El Coloradito fault zone is a ~4 km wide zone of ENE-striking faults transecting the central Sierra San Fermín (Fig. 3). The exposed length of the fault zone is ~15 km. There are two sets of principal structures in the El Coloradito fault zone: an older set of E- to ENE-striking, mostly S-dipping faults with both dip-slip and strike-slip striae, and a younger set of NE- to N-striking normal or sinistral normal faults. Normal faulting began in the El Coloradito fault zone between 12.5 and 6 Ma, and exerted a strong control on the distribution and thickness of late Miocene tuffs (Lewis, 1994; updated by geochronology of Stock *et al*., 1997). Dip discordances between tuffs of Group 3 indicate active westward tilting at about 6 Ma. Middle to late Pliocene ash-flow tuffs and sedimentary strata (Groups 4 and 5) have been tilted westward at least 12–15°. Normal faults became reactivated as sinistral faults about 3 Ma and are active today (Lewis, 1994). Thus the sinistral shear component of strain clearly increased in Pliocene time.

We reconstructed the amount of sinistral separation across the El Coloradito fault zone using as piercing points the fault cutoffs of the angularly discordant contact between two Group 3 tuffs. We computed ~6 km of cumulative sinistral slip since deposition of these 6 Ma tuffs (a rate of approximately 1 mm/y). Because sinistral separation may be enhanced by the low angle of the discordance, the westward dips of the units, and erosion of the contacts, 6 km is an upper bound.

Dead Battery Canyon fault. The Dead Battery Canyon fault is a major, NNE-striking, moderately to steeply E-dipping, normal fault (Fig. 3). It offsets tuffs of Group 3 ~550 m down to the east. The Dead Battery Canyon fault either terminates southward by bending westward into the El Coloradito fault zone, or it is cut off by this fault zone and offset in a sinistral sense. The Dead Battery Canyon fault dies northward as displacement steps right onto an unnamed, subparallel, E-dipping normal fault. This fault in turn appears to transfer displacement onto the NW-dipping Ironwood Canyon fault.

The youngest faults in the Dead Battery Canyon area are ENE-striking sinistral faults which form shutter ridges and control drainages (Lewis, 1994). Many of these faults cut Pliocene, and in some cases Quaternary, alluvial deposits. Many NNE-striking fault planes also cut Pliocene sedimentary rocks (Group 5). These faults have small (centimeter-scale), dip-slip offsets down to the west. Abundant NE-striking faults, possibly Riedel shears, cut Group 5 rocks as well. These three fault sets (ENE-, NNE-, and NE-striking) are kinematically related to the major sinistral shear zone that extends through the El Coloradito/Dead Battery Canyon area.

Depositional patterns indicate that faulting in the Dead Battery Canyon area began at least by about 6 Ma, prior to deposition of the late Miocene tuffs of Group 3. Westward tilting of fault blocks caused angular discordances between Group 3 tuffs and westward thickening of some units. The primary controls on depositional patterns appear to have been major down-to-the-east normal faults which tilted fault blocks in this area westward towards the Sierra San Felipe fault. These faults do not appear to have been active into Pliocene time. After explosive volcanism

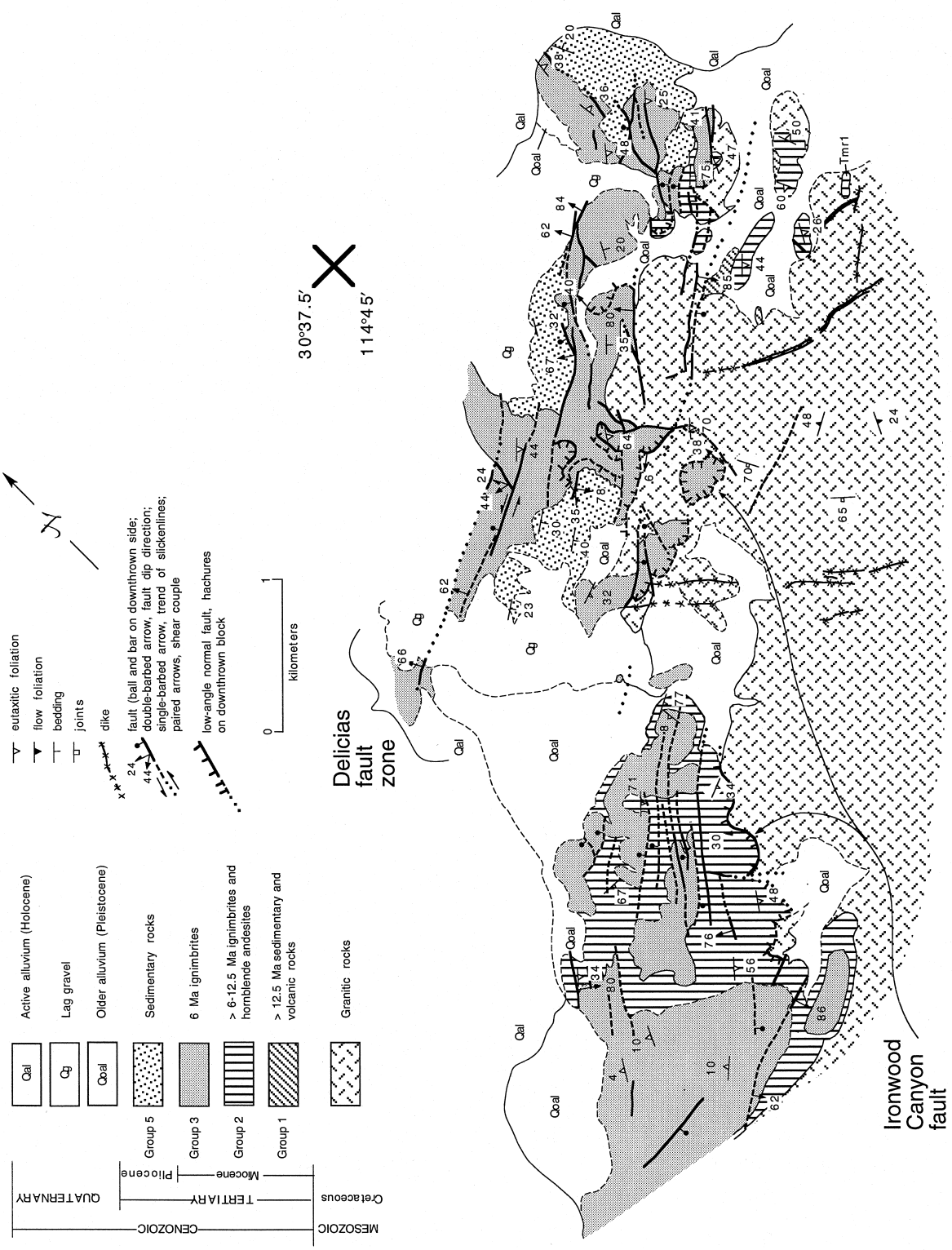

Fig. 6. Detailed geologic map of the Ironwood Canyon fault zone.

abated in Pliocene time, the basin south of Dead Battery Canyon continued to fill with lacustrine (or marine) and alluvial sediments.

Structural summary. Extension began in the Sierra San Fermín–southern Sierra San Felipe between 12.5 and 6 Ma, producing three major normal fault systems, the E-dipping Sierra San Felipe fault, the NW-dipping Ironwood Canyon detachment fault, and the S-dipping El Coloradito fault zone. Domino faulting in the Ironwood Canyon fault zone lasted from late Miocene time (about 6 Ma) into Pliocene time, creating a supradetachment basin which preserves a thick section of latest Miocene/Pliocene lacustrine or marine mudstones and alluvial conglomerates. Normal faulting characterized the structural style in late Miocene time. This style changed in Pliocene time to a combination of normal faulting and sinistral strike slip, the latter in some cases reactivating reoriented normal faults. We infer that both the El Coloradito and Delicias fault zones are now secondary sinistral faults within the dextral transcurrent plate boundary zone in the northern Gulf region. Similar zones of sinistral slip in areas as much as 100 km north of the study area (Hamilton, 1971; Andersen, 1973; Boehm, 1984; Bryant, 1986; Stock *et al*., 1996) are probably related (Fig. 2).

Amounts of extension

In order to compute the amount of extension in the southern Sierra San Felipe and Sierra San Fermín, we restored displaced marker horizons along several sections that traverse the hanging wall of the Ironwood Canyon fault (El Coloradito fault zone and northern Sierra San Fermín), the hanging wall of the Sierra San Felipe fault (western Sierra San Fermín), and the El Coloradito fault zone (Fig. 7). Within each line of section, we used the most continuous unit in the stratigraphic section as the structural marker, Miocene basalt Tmb in A–A′; 12.5 Ma Tuff of San Felipe (Tmsf) and 6 Ma Tmr3 in B–B′; and 6 Ma Tmr3 in C–C′. Extension varies from 6–7% in the hanging wall of the Ironwood Canyon fault (A–A′ and western part of B–B′) and 8% in the western Sierra San Fermín (C–C′) up to 24% in the northern Sierra San Fermín (eastern part of B–B′). The amount of extension is as high as 42% locally within the El Coloradito fault zone (Lewis, 1994). The Tuff of San Felipe everywhere dips more steeply than the 6 Ma Tmr3, and must have undergone extension between 12.5 and 6 Ma. Because the Tuff of San Felipe is largely buried throughout the Sierra San Fermín, and Tmr3 is discontinuously preserved in the Sierra San Felipe, we cannot directly compare amounts of extension in the units in order to evaluate changes in the rate of extension, as predicted by plate reconstructions (Stock and Hodges, 1989). Field relations show that most normal separation on major normal faults, and most domino faulting, occurred post-6 Ma.

Fault geometries at depth

Geometric constraints allow the Sierra San Felipe fault to be either planar or curved beneath the Sierra San Fermín. The westward tilt of the homoclinal block (Fig. 3) does not require a curved fault as no rollover of bedding attitudes has been identified further east in the Sierra San Fermín.

The consistency of paleomagnetic declination anomalies in the hanging walls of the Sierra San Felipe and Ironwood Canyon faults suggests that they are kinematically linked and may root into, and rotate on, the same detachment fault (Lewis and Stock, in press). Eastward dips in Miocene volcanic rocks in the northern Sierra San Fermín, within both hanging wall and footwall of the Ironwood Canyon detachment fault, suggest that a deeper detachment underlies and dips northwestward beneath the Sierra San Fermín, accounting also for eastward dips in Pliocene marine rocks on the east side of the Sierra San Fermín. Alternatively, structures may root into an eastward extension of the San Pedro Mártir fault, which might ramp down to a lower detachment level beneath this area, accounting for the preponderance of westward-dipping (antithetic) faults and eastward-dipping strata.

PALEOSTRESS ORIENTATIONS AND MAJOR EPISODES OF FAULTING

Inversion method

We apply an inverse method devised for determining regional stresses from populations of fault/slickenline data [Fault Mechanism Stress Inversion (FMSI); Gephart and Forsyth, 1984; Gephart, 1990a,b]. This method searches for a stress tensor which minimizes the discrepancy between the predicted shear stress direction and the observed slip direction on each fault plane. Because slip is assumed to occur in the direction of resolved shear stress (Bott, 1959), no assumptions are made regarding the orientation of a fault plane relative to the stress tensor. A robust solution can be obtained even if weak faults, formed in previous tectonic events, are included in the analysis.

The inversion yields an estimate of four model parameters, the best-fitting principal stress directions and a measure of relative stress magnitudes R, where

$$R = (\sigma_2 - \sigma_1)/(\sigma_3 - \sigma_1). \quad (1)$$

$R = 0$ if $\sigma_2 = \sigma_1$, and $R = 1$ if $\sigma_2 = \sigma_3$. The best-fitting model is found by applying a grid search over the four parameters by systematically varying each parameter over a specified range of possibilities (see detailed

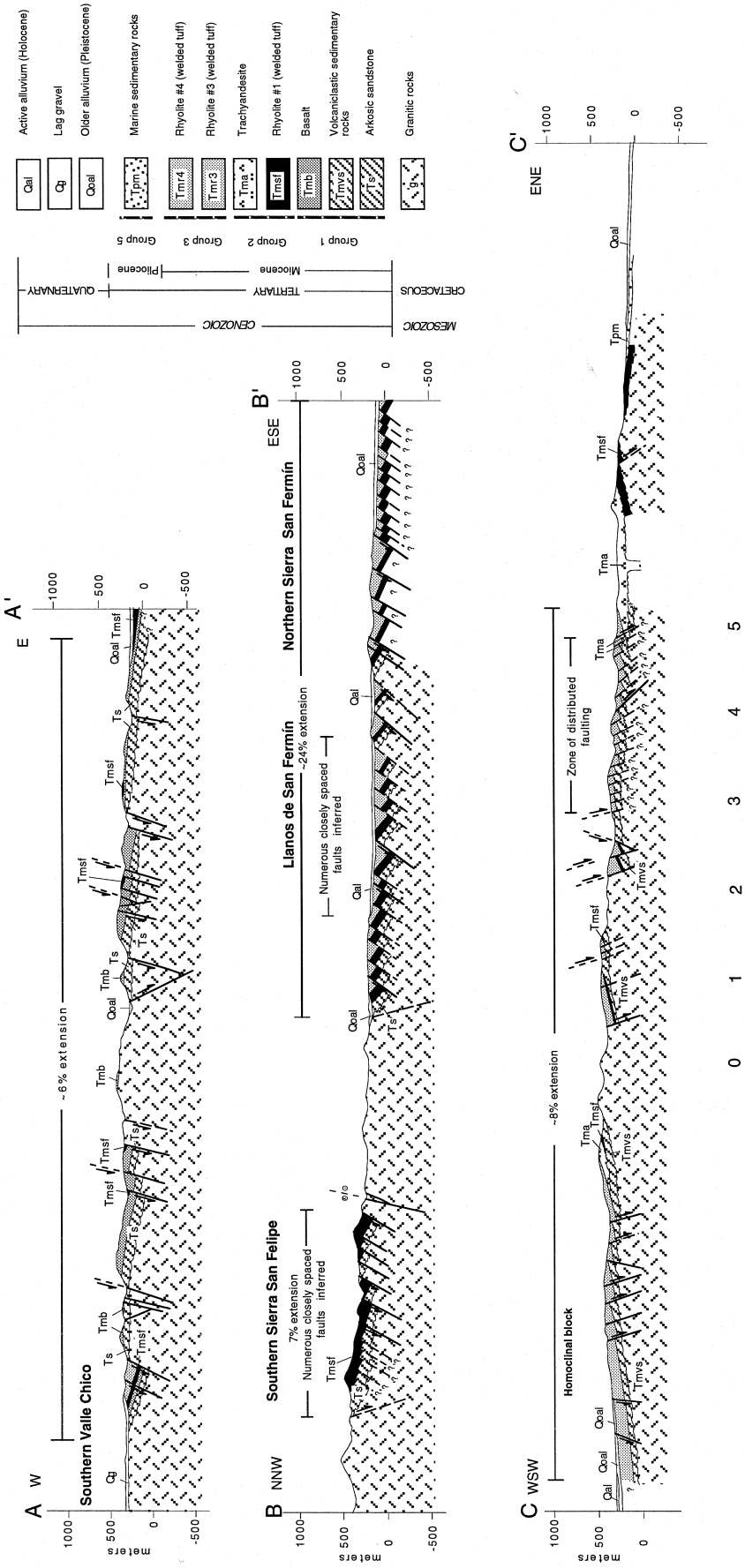

Fig. 7. Cross-sections of Sierra San Fermín/Sierra San Felipe area. Cross-section lines as in Fig. 3. Dips of some faults could not be measured or inferred from the map pattern (because covered with alluvium), but were assumed to be parallel to those nearby. We also assumed high fault-to-bedding cutoff angles, consistent with near vertical cutoff angles along section lines. No assumptions were made regarding the geometry of the basal detachment faults (listric or planar).

development in Gephart and Forsyth, 1984; Gephart, 1990a, b). The measure of misfit is given by the smallest rotation about an axis of any orientation that brings the fault plane/slip vector into an orientation consistent with the stress model. For each stress model constructed, the magnitudes of the misfits for all fault data are summed (as absolute values) to achieve a measure of fitness of the model, and the model with the smallest sum of misfits is the best-fitting model. Confidence limits defining the acceptable range of models are then constructed using statistical methods for a one-norm measure of misfit (based on Parker and McNutt, 1980), which reduces the influence of extreme data by minimizing the sum of the absolute values of the misfits rather than the sum of the squares of the misfits. Confidence limits correspond to contours of equal misfit in four-dimensional (three stress directions and R) space, giving a realistic measure of the uncertainty in the analysis.

The implicit assumptions of this method, and other methods that invert fault/slickenline data to obtain the regional stress tensor, are that: (1) stress in the region is spatially and temporally uniform and all slip events reflect a common stress field, (2) slip is assumed to occur in the direction of resolved shear stress, and (3) strain is coaxial with stress. In the first case, field observations can be used to minimize effects of stress fields that change through time. If more than one tectonic event has occurred in the area, a separation of the data into two or more groups corresponding to the different events must be made prior to running the inversion, as we have done here. An additional complication results if faults and their slip indicators have been reoriented significantly, within a constant stress field, subsequent to faulting. Because Group 1 faults have been affected by vertical-axis block rotations, this assumption may not strictly hold for the data here. In the second case, fault interactions or block interactions may influence the local stress field, producing striae that do not represent the resolved direction of *regional* shear stress on the fault plane; these data may therefore produce a poor fit (Pollard *et al*., 1993). This assumption could be violated in the present study area because the two principal sets of active faults may interact mechanically. However, the low to moderate spatial density of faults in much of the study area and the short length of most faults suggest that fault interactions do not appreciably affect the stress tensor computed by the inversion. Assumption (3) is generally true in the present study area because deformation, characterized by mixed strike-slip and dip-slip, appears dominated by pure shear. However, comparison of models derived from grid-search stress inversion and graphical kinematic analysis (e.g. Marrett and Allmendinger, 1990) can show whether non-coaxial strain has produced measurable differences between stress and strain axes.

Results of inversion

As a starting point for our inversion, we inspected the scatter in extension directions in our two data groups using graphical methods of kinematic analysis (Angelier and Mechler, 1977; Marrett and Allmendinger, 1990). We established, for both Groups 1 and 2, that the preferred extension axis is roughly horizontal and trends W–E, whereas the shortening axes form a roughly N–S girdle on an equal area projection.

Using an approximate version of the FMSI method (Gephart and Forsyth, 1984; Gephart, 1990a), we then performed a preliminary grid search of about 5000 stress models with the σ_3 axis roughly horizontal and W–E-trending. For each σ_3 axis, we inspected models covering a broad range of σ_1 and σ_2 axes within the plane normal to the σ_3 direction. Confidence limits around the best-fitting models indicated that the σ_3 axis lay nearly horizontal and W–E for Group 1, and nearly horizontal and WSW–ENE for Group 2. These axes are within the error limits of each other.

Using the exact method, we searched for the best models among 5000 models covering the range of the 68% confidence interval determined by the initial approximate search. The results of our exact search are shown in Fig. 8. We then examined our best-fitting models for each group and acceptable alternative models to see if we could eliminate either strike-slip or extensional models because of inconsistency with a reasonable failure criterion (Byerlee's Law; Byerlee, 1978). Mohr diagrams for the alternative models are shown in Fig. 9.

In the optimum stress model for Group 1, σ_3 plunges 0° in a WSW direction (261°) and σ_1 is approximately vertical, suggesting an extensional faulting regime. However, the range of acceptable models includes both normal and strike-slip stress tensors (Fig. 8). In fact, the value of $R = 0.9$ in the best-fitting model indicates that σ_2 and σ_3 are nearly equal, consistent with the numerous E-striking normal faults in this data set. Mohr diagrams, however, show a large number of faults with low shear stress and low normal stress for both extensional and strike-slip models, including some of the E-striking normal faults (Fig. 9). It is possible that the slip indicators in these fault planes pertain to an earlier tectonic event, prior to reorientation by ~30° of vertical-axis rotation from original northeasterly strikes (Lewis and Stock, in press).

In the best-fitting model of Group 2 data, σ_3 plunges 23° towards 243° and σ_1 plunges 48° towards 001°, indicating a combined normal/strike-slip or transtensional stress regime with a WSW–ENE direction of least principal stress (Fig. 8). For stress models within the 95% confidence limit, σ_1 axes form a girdle on the equal area projection. This is consistent with the mixture of dip-slip and strike-slip Pliocene to Quaternary

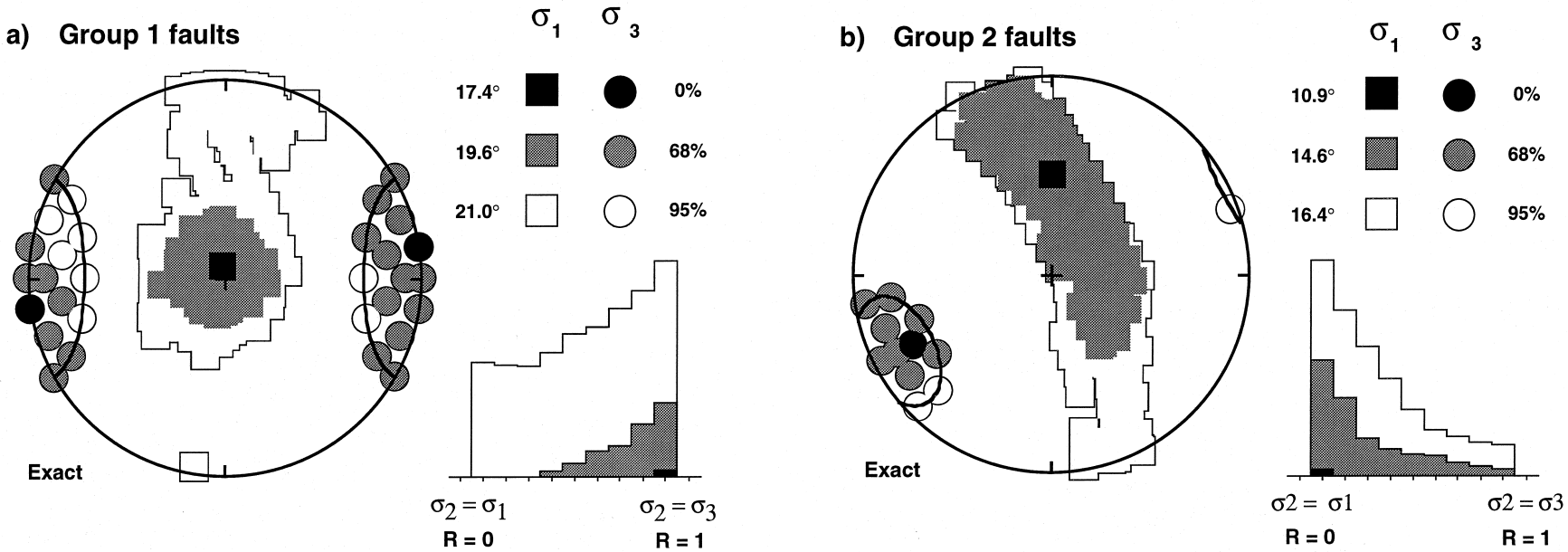

Fig. 8. Equal area, lower hemisphere projections of σ_1 and σ_3 directions and histograms of R values indicating the range of acceptable stress models for (a) Group 1 faults ($N = 91$) and (b) Group 2 faults ($N = 27$) from the Sierra San Fermín study area. Boxes (circles) indicate σ_1 (σ_3) directions; each stress direction shown on the plot corresponds to at least one stress model. The grid search was performed about the axis estimated to have the smaller uncertainty (as suggested by tighter clustering of T axes in preliminary graphical analysis using the method of Marrett and Allmendinger, 1990); for both groups, σ_3 was selected as the primary principal stress. σ_3 directions were set by a predefined grid (10° spacing) within a prescribed range (30° for Group 1 and 14° for Group 2) about the initial estimate of σ_3. In the plane orthogonal to σ_3, several secondary stress directions (σ_1) were tested. The average misfit value (see text for discussion) associated with each confidence limit is given at the upper right; the best-fitting model in each case is indicated by '0%'. All data in Groups 1 and 2 are consistent to within a 20° rotation with at least one of the stress models within the 68% confidence limit for that Group. Thus these stress models appear to be reasonably good fits. Histograms indicate the number of models found within each confidence limit for each value of R.

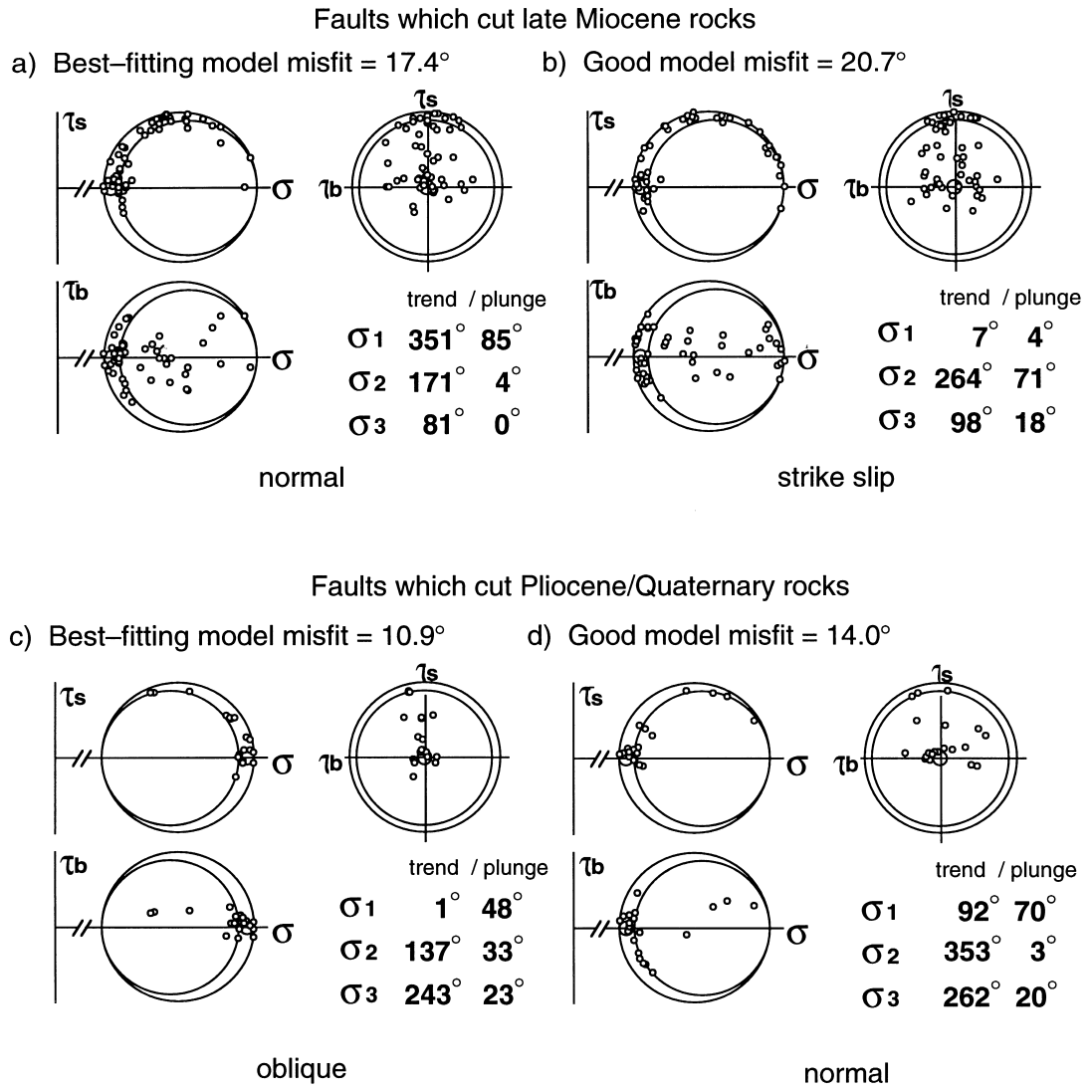

Fig. 9. Paired Mohr diagrams for two stress models fitting fault/slickenline data within the 95% confidence limit, illustrating the general consistency of our results with a reasonable failure criterion. Three orthogonal views of the Mohr sphere for stress are illustrated. τ_s and τ_b are components of shear stress. Each circle shows a fault geometry (a pole to a fault plane with associated slip direction) relative to the three principal stress directions. Fault geometries consistent with a reasonable failure criterion plot on the circles or within the area between the largest circle and the two smaller ones on the [$\tau_s > 0$, $\tau_b = 0$] half-plane of the Mohr Sphere. Only faults with misfits less than 20° are shown. The normal model for Group 1 has fewer faults with low shear stress/high normal stress than the strike-slip model and therefore represents the better model. The normal model for Group 2 is more consistent with a reasonable failure criterion than the best-fitting, oblique model (see text for discussion).

faults observed in the field. The large number of both extensional and strike-slip stress models within the 95% confidence limit suggests that σ_1 and σ_2 are nearly equal, as noted for Pliocene rocks of the Santa Rosalía area, southern Baja California (Ortlieb *et al.*, 1989). We infer that σ_1 must have been vertical at least in some areas or at some times because of the prevalence of normal faults. An extensional model for Group 2 data is consistent with a reasonable failure criterion (Fig. 9), suggesting the continuing importance of extension in this area into Quaternary time. The value of $R = 0.1$ in our best-fitting model, as well as many other acceptable models, implies a component of NNW–SSE compression. Geodetic data show a small, modern-day component of N–S shortening across the central Gulf (Ortlieb *et al.*, 1989), consistent with our results.

The results of this analysis provide some insight into applicability of assumption (2) that slip occurs in the direction of resolved shear stress. All data in Groups 1 and 2 are consistent to within a 20° rotation with at least one of the stress models within the 68% confidence limit for that Group. Because these misfits are not large compared to modeled discrepancies between the direction of slip and the direction of maximum shear stress drop for fault interactions (Pollard *et al.*, 1993), we suggest that fault interactions do not appreciably affect the computed stress tensor.

In summary, inversion of kinematic data shows that the axis of least principal stress was oriented WSW–ENE in Pliocene/Quaternary time and perhaps in late Miocene time as well. The results of our inversion, which overlap within uncertainties for Group 1 and 2 fault sets, are consistent with field relations, which indicate that normal faulting characterized the structural style in late Miocene time, but that this style changed in late Pliocene time to sinistral oblique faulting. Distributed dextral shear has clearly been important in Pliocene to Recent time, with the best-fitting stress model indicating a transtensional regime in which σ_1 and σ_2 are nearly equal, with σ_1 likely to alternate between horizontal and vertical. The mixture of acceptable models of Group 1 data with σ_1 horizontal as well as vertical suggests that dextral shear may have played a role in late Miocene time, but we cannot distinguish whether this is the original late Miocene signature or a Pliocene to Recent overprint. Another complicating factor is paleomagnetic evidence for $\sim 30^\circ$ of clockwise vertical-axis rotation since 6 Ma (Lewis and Stock, in press). Restoring the late Miocene direction of least principal stress suggests a direction between W–E and SW–NE for this interval. This range includes the 230° direction of extension predicted by plate reconstruction models for the Gulf Extensional Province in late Miocene time (Stock and Hodges, 1989). The late Miocene results should be interpreted cautiously, however, because of the likelihood that late Miocene faults were reoriented and reactivated, perhaps repeatedly, during clockwise rotation (e.g. Scotti *et al.*, 1991).

DISCUSSION

A comparison of our results with stress and strain analysis reported for other areas in the Gulf Extensional Province reveals significant similarities as well as temporal and spatial differences, which may derive in part from varying uncertainties in age constraints but also local differences in strain partitioning within the plate boundary zone. Fault/slickenline data from the Santa Rosalía and Loreto areas in northern Baja California Sur indicate a SW–NE minimum stress for faults that cut latest Oligocene to middle Miocene rocks (Angelier *et al.*, 1981, updated by geochronology of Hausback, 1984 and Sawlan and Smith, 1984; Zanchi, 1994). Faults in Pliocene strata record a small clockwise reorientation of the minimum stress to a WSW–ENE direction in the Santa Rosalía area (Angelier *et al.*, 1981), and a W–E direction in the Loreto area (Zanchi, 1994). Numerous dextral and dextral oblique faults, in addition to dip-slip faults, cut Pliocene rocks in these two areas. The regional late Pliocene extension direction for southern Baja California (determined by kinematic analysis) appears to be W–E with a slight dextral component (Umhoefer and Stone, 1996). In northern Baja California, W–E extension occurred between ~16 and 11 Ma in Arroyo Grande, about 100 km north of the present study area (kinematic analysis; Lee *et al.*, 1996). Minor sinistral oblique slip occurred on some faults in Arroyo Grande. In the southern Valle Chico area, WSW–ENE extension was estimated from the dominant strikes of faults in middle–late Miocene rocks (Stock and Hodges, 1989). Within the area studied here, the stress regimen appears to have been dominantly extensional with least principal stress oriented between W–E and SW–NE in late Miocene time and dextral oblique with a WSW–ENE minimum stress during Pliocene to Recent deformation. The 95% confidence limits on our least principal stress axes encompass all the published least principal stress or strain axes cited above from northern and southern Baja California, suggesting that small changes in stress and strain axes may not be resolvable when realistic uncertainties are applied. The combined results of our geometric analysis and stress inversion indicate an important change in the amount of dextral shear, but not necessarily the least principal stress direction, at about 3 Ma.

The onset of normal faulting in the Sierra San Fermín–Sierra San Felipe and progressive changes in the geometry of faulting through time are consistent with regional strain partitioning within the Pacific–North America plate boundary zone, although significant uncertainties remain with respect to the timing of vertical-axis rotations, sinistral faulting, and the reorientation in the direction of relative plate motion. Extension began in the Sierra San Fermín–southern Sierra San Felipe between 12.5 and 6 Ma, consistent with onset of extension in other areas in northeastern Baja California (Stock and Hodges, 1990; updated by geochronology of Stock *et al.*, 1997; Lee *et al.*, 1996). Least principal stress was oriented between W–E and SW–NE in late Miocene time. Middle–late Miocene onset of extension, with a least principal stress of this direction, supports global plate reconstructions that show markedly oblique plate motion for an interval in Miocene time that may have been 10.5–5.5, 15–7, or 9–5 Ma (Stock and Hodges, 1989). In this early period of Gulf rifting, strain was partitioned between two active belts of deformation, the San Benito–Tosco–Abreojos strike-slip fault zone (SBTAFZ), in the Pacific margin west of the peninsula, and the obliquely rifting Gulf Extensional Province (Hausback, 1984; Stock and Hodges, 1989). From ~6.5 to ~3 Ma, locally intense extensional faulting and volcanism, and the onset of vertical-axis block rotations (Lewis and Stock, in press) in the Sierra San Fermín–southern Sierra San Felipe suggest important changes within the plate boundary zone. This period from latest Miocene to early Pliocene might correspond to a transitional stage of Gulf development (~6–3.5 Ma; Lonsdale, 1989; Umhoefer *et al.*, 1994). By this time, the Pacific and North American plates had assumed their modern

direction of relative displacement (Stock and Hodges, 1989), and the Baja California peninsula was isolated between the developing transform–rift system in the Gulf region and the still-active SBTAFZ along the Pacific margin (Lonsdale, 1989). In the last ~3 My, structural constraints indicate significant sinistral slip in the Sierra San Fermín and continuing vertical-axis rotations (Lewis and Stock, in press). This late Pliocene increase in shear may correspond to the beginning of the modern Gulf stage (3.5–0 Ma; Lonsdale, 1989; Umhoefer *et al.*, 1994), during which virtually all relative plate displacement has been accommodated within the Gulf region. Strain has been partitioned in this period, within the northern Gulf region, between obliquely rifting northeastern Baja California and the transform–rift system in the Gulf itself.

Comparison with physical models of oblique rifting

The structural geometry and kinematics observed in the study area support the predictions of physical and analytical models of oblique rifting (Fig. 10; Withjack and Jamison, 1986; Tron and Brun, 1991; Teyssier *et al.*, 1995). When the Main Gulf Escarpment, the western boundary of the Gulf Extensional Province, began

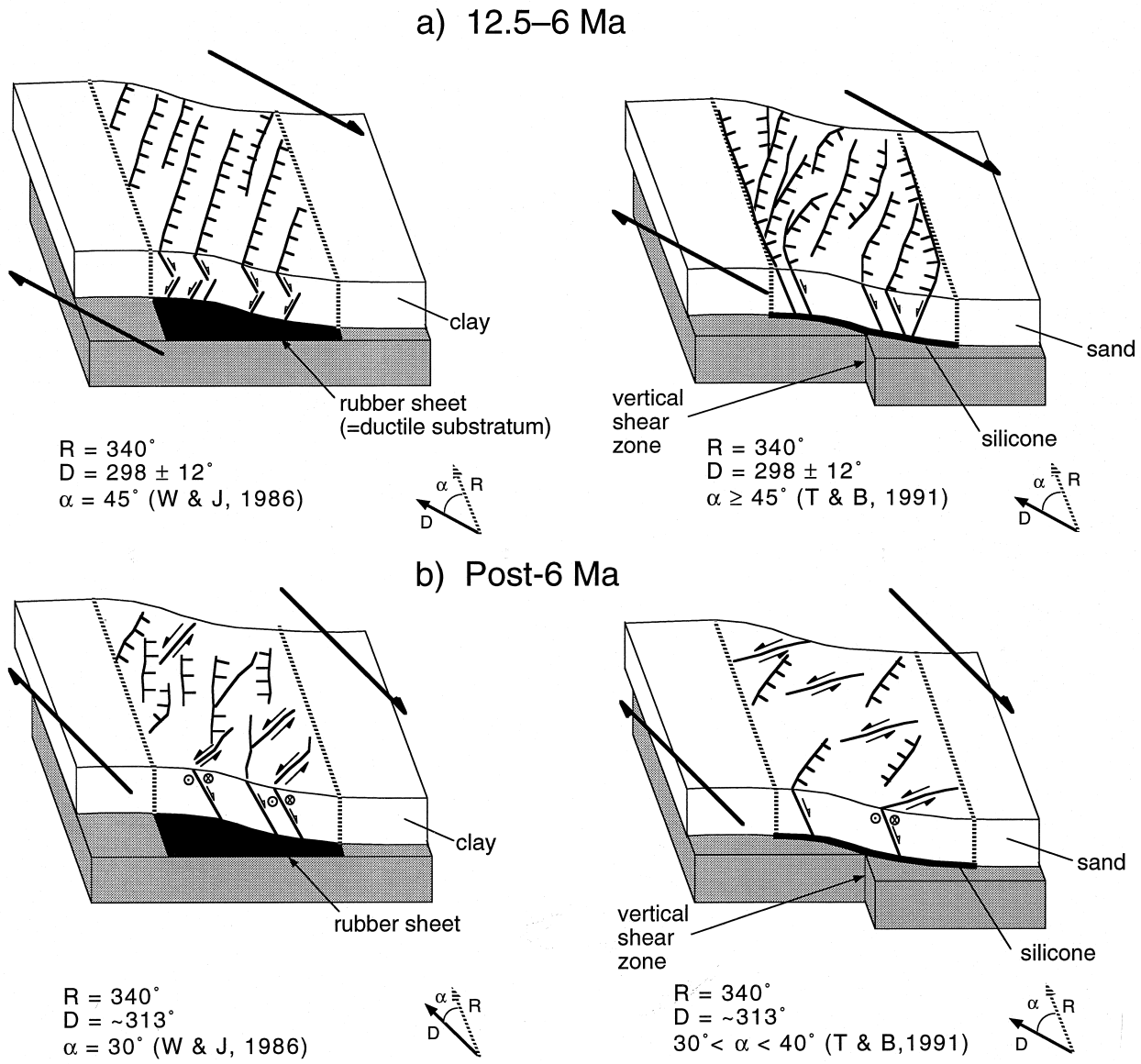

Fig. 10. Block models of oblique rifting applied to northeastern Baja California. *R*, rift trend; *D*, direction of relative plate displacement; α, angle between direction of relative motion and bounds of the deforming zone. Dashed lines mark rift trend and bounds of deforming zone. Faults: hachured lines are normal faults, with hachures on downthrown block; lines with two single-barbed arrows are strike-slip faults. Small, open, single-barbed arrows, circles with dots, and crossed circles indicate dip-slip movements, outward movements, and inward movements, respectively. Large, single barbed arrows indicate direction of relative plate displacement. Block models based on physical and analytical models of Withjack and Jamison (1986) and Tron and Brun (1991).

forming in northeastern Baja California, its north-northwesterly strike formed an angle of ~30–55° to the direction of relative plate motion (298° ± 12°; Stock and Hodges, 1989). This case is similar to clay models in which the orientation of the stretching vector α, the angle between the direction of shear and the bounds of the deforming zone (i.e. the San Pedro Mártir fault, striking ≈340°), is equal to or greater than 45° (Withjack and Jamison, 1986; Tron and Brun, 1991). In clay models of Withjack and Jamison (1986), displacement is applied along a basal zone of finite width, simulating a horizontal velocity discontinuity or décollement at the base of the crust. Where $\alpha = 45°$, primarily normal faults, striking ~40° clockwise of the rift trend, are produced. By analogy, normal faults in northeastern Baja California would have originated at strikes of about 020°, matching reasonably well the restored strikes of late Miocene normal faults which have been rotated clockwise about a vertical axis (e.g. Ironwood Canyon detachment fault and El Coloradito fault zone).

The 'modern' direction of relative motion between the Pacific and North American plates at about 30°N latitude is 313° (NUVEL-1 global plate-motion model; DeMets *et al.*, 1990), 314° (kinematic model; Humphreys and Weldon, 1991), or 303–312° (earthquake slip vector azimuths from events within the Gulf of California; Goff *et al.*, 1987). The change to the modern direction at about 5 Ma (Stock and Hodges, 1989) suggests a change to an $\alpha \approx 25$–$35°$. Where $\alpha = 30°$ (experiments were run for α from 0 to 90° in 15° steps), clay models indicate a greater component of dextral shear accommodated by two sets of faults, normal faults with strikes of about 005° and sinistral-slip faults with strikes of about 040° (Fig. 10). These orientations are quite consistent with strikes and sense of slip of Quaternary faults in the study area.

In the sand–silicone experiments of Tron and Brun (1991), displacement is applied along a narrow line at the base of a silicone layer rather than a basal zone of finite width as in the experiments of Withjack and Jamison (1986). This class of models simulates a vertical shear zone, or velocity discontinuity, in strong upper mantle beneath ductilely deforming lower crust and brittle upper crust (Fig. 10). For low-obliquity rifting, where $\alpha \geq 45°$, curved faults are common, with displacement varying from dip-slip to strike-slip along them. A small percentage of faults form parallel to the deforming zone, along its margins, whereas most faults form oblique to the margins. This is similar to the geometry observed in northeastern Baja California, where the Main Gulf Escarpment and the Valle de San Felipe fault parallel the rift trend, but faults to the east are oblique. We might expect those faults oblique to the bounds of the deforming zone to rotate as deformation progresses.

For high-obliquity rifting, where $\alpha < 45°$, distinct sets of dip-slip and strike-slip faults form (Fig. 10). Where α is between 30 and 45°, oblique-slip faults form 65–75° to the stretching vector, whereas strike-slip faults are oriented 50–65° to the stretching vector. This is similar to the late Pliocene/Quaternary geometry in the study area, where oblique-slip faults strike from about 045° to 055° (northeasterly) and strike-slip faults from 055° to 070° (east-northeasterly). However, this model does not predict the numerous normal faults with north-northeasterly strikes. The Tron and Brun (1991) models do correctly predict the dominance of normal faults early in the development of the GEP ($\alpha \geq 45°$), and the increasing importance of strike-slip faults and vertical-axis rotations as the direction of relative plate motion became less oblique ($\alpha < 45°$).

The similarity between physical and analytical models of oblique rifting and map-scale structures in northeastern Baja California suggest that oblique rifting is a reasonable explanation for the development of these structures, as previously suggested for the Gulf of California as a whole (Withjack and Jamison, 1986) and for regions within it, including the Loreto basin (Umhoefer and Stone, 1996) and Arroyo Grande (Lee *et al.*, 1996).

CONCLUSIONS

Normal faulting began in the Sierra San Fermín–southern Sierra San Felipe between 12.5 and 6 Ma, producing the N-striking Sierra San Felipe fault and the NE-striking Ironwood Canyon and El Coloradito fault zones. The latter are presently oriented ENE, following ~30° of clockwise vertical-axis rotation in the Sierra San Fermín. The Sierra San Felipe and Ironwood Canyon normal faults are kinematically linked and presumed to sole into a deeper detachment, perhaps the eastward continuation of the San Pedro Mártir fault.

Most extension occurred within the study area post-6 Ma, judging by the small angular discordance (< 5°) between 12.5 and 6 Ma tuffs, and much greater tilting since 6 Ma. Extension is generally < 10% in 6 Ma rocks and somewhat more in 12.5 Ma rocks, although late Miocene strata are extended up to 42% locally. Most of the normal separation on major faults in the area developed post-6 Ma. The steep eastern escarpment of the Sierra San Felipe developed post-6 Ma, but became inactive not long afterwards. Vertical-axis block rotations began post-6 Ma as well. Normal faulting in the El Coloradito fault zone strongly affected thickness and distribution of 6 Ma tuffs, and marine sedimentation began there shortly after 6 Ma. Domino faulting in the Ironwood Canyon fault zone was most intense between about 6 and 3 Ma. By about 3 Ma, the El Coloradito and Ironwood Canyon fault zones were accommodating sinistral slip. By that time, combined normal and sinistral faulting and vertical-axis block rotations accommodated distributed dextral

shear within this part of the Gulf Extensional Province.

Inversion of kinematic data indicates a minimum stress direction between W–E and SW–NE in late Miocene time and a WSW–ENE direction in Pliocene/Quaternary time, but the late Miocene results are complicated by vertical-axis block rotations and fault reactivation and therefore must be interpreted cautiously. A small component of dextral shear may have played a role in late Miocene time, but we cannot distinguish whether this is the original late Miocene signature or a Pliocene to Recent overprint. Dextral shear has clearly been important in Pliocene to Recent time, with the best-fitting stress model indicating a transtensional regime in which σ_1 and σ_2 are nearly equal with σ_1 probably alternating between horizontal and vertical. The results of our inversion are consistent with field relations, which indicate that normal faulting characterized the structural style in late Miocene time but that this style changed in late Pliocene time to combined normal and sinistral faulting.

Progressive changes in the geometry of faulting through time are consistent with regional strain partitioning within the Pacific–North America plate boundary zone, and are predicted by physical and analytical models of oblique divergence as the orientation of the stretching vector α changes to lower and lower values. The structural evolution of this area supports the idea that the transfer of Baja California from the Pacific to the North American plate was a gradual process, beginning not long after the initiation of transform faulting in the Pacific margin, with important changes in the geometry and kinematics of plate motions and deformation within the plate boundary about 6 My ago and about 3 My ago.

Acknowledgements—This research was partially supported by National Science Foundation grants EAR-89-04022 and EAR-92-18381 and a Presidential Young Investigator Award (EAR-90-58217/EAR-92-96102) to Joann M. Stock. Additional support was provided to Claudia Lewis by the Harvard University Department of Earth and Planetary Sciences Grants-in-Aid for Fieldwork. We thank John Gephart for his generosity in allowing us to use his computer program FMSI for inverting fault/slickenline data, Rick Allmendinger and Randy Marrett for use of FaultKin, and the Division of Earth and Planetary Sciences at the California Institute of Technology for many resources necessary for completion of this project. We are grateful to Josephine Burns, Cheryl Contopulos, Tim Johnson, Dan Reilly, Chris Small, and Susan Turbek for assistance in the field and to Mark Abolins, Gary Axen, Jeff Lee, Arturo Martín Barajas, Tim Melbourne, Elizabeth Nagy, Zeke Snow, and Leslie Sonder for many helpful discussions. We thank Richard Norris and two anonymous referees for constructive reviews which greatly improved the manuscript.

REFERENCES

Allen, C. R., Silver, L. T. and Stehli, F. G. (1960) Agua Blanca fault—A major transverse structure of northern Baja California, Mexico. *Geological Society of America Bulletin* **71,** 457–482.

Andersen, R. L. (1973) Geology of the Playa San Felipe quadrangle, Baja California, Mexico. M.S. thesis. California State University, San Diego.

Angelier, J., Colletta, B., Chorowicz, J., Ortlieb, L. and Rangin, C. (1981) Fault tectonics of the Baja California peninsula and the opening of the Sea of Cortez, Mexico. *Journal of Structural Geology* **3,** 347–357.

Angelier, J. and Mechler, P. (1977) Sur une méthode graphique de recherche des contraintes principales également utilisable en tectonique et en seismologie: La méthode des diedres droits. *Bulletin de la Société Géologique de France* **19,** 1309–1318.

Axen, G. (1995) Extensional segmentation of the Main Gulf Escarpment, Mexico and United States. *Geology* **23,** 515–518.

Boehm, M. (1984) An overview of the lithostratigraphy, biostratigraphy, and paleoenvironments of the late Neogene San Felipe marine sequence, Baja California, Mexico. In *Geology of the Baja California Peninsula*, ed. V. A. Frizzell, pp. 253–266. Society of Economic Paleontologists and Mineralogists, Pacific Section, Los Angeles, **39**.

Bott, M. H. P. (1959) The mechanics of oblique slip faulting. *Geological Magazine* **96,** 109–117.

Brown, L. G. (1978) Recent fault scarps along the eastern escarpment of the Sierra San Pedro Mártir, Baja California. M.S. thesis, San Diego State University.

Bryant, B. A. (1986) Geology of the Sierra Santa Rosa basin, Baja California, Mexico. M.S. thesis. San Diego State University.

Byerlee, J. (1978) Friction of rocks. *Pure and Applied Geophysics* **116,** 615–626.

Curray, J. R. and Moore, D. G. (1984) Geologic history of the mouth of the Gulf of California. In *Tectonics and Sedimentation along the California Margin*, eds J. K. Crouch and S. B. Bachmann, pp. 17–36. Society of Economic Paleontologists and Mineralogists, Los Angeles, California, **38**.

DeMets, C., Gordon, R. G., Stein, S. and Argus, D. F. (1987) A revised estimate of Pacific–North America motion and implications for western North America plate boundary zone tectonics. *Journal of Geophysical Research* **93,** 11,877–11,897.

DeMets, C., Gordon, R. G., Argus, D. F. and Stein, S. (1990) Current plate motions. *Geophysical Journal International* **101,** 425–478.

Dokka, R. K. and Merriam, R. H. (1982) Late Cenozoic extension of northeastern Baja California. *Geological Society of America Bulletin* **93,** 371–378.

Fenby, S. S. and Gastil, R. G. (1991) Geologic–tectonic map of the Gulf of California and surrounding areas. In *The Gulf and Peninsular Province of the Californias*, eds J. P. Dauphin and B. R. T. Simoneit, pp. 79–83. American Association of Petroleum Geologists Memoir, **47**.

Gastil, G., Lemone, D. and Stewart, W. (1973) Permian fusilinids from near San Felipe, Baja California. *American Association of Petroleum Geologists Bulletin* **57,** 746–747.

Gastil, G., Morgan, G. and Krummenacher, D. (1981) The tectonic history of peninsular California and adjacent Mexico. In *The Geotectonic Development of California*, ed. W. G. Ernst, Rubey Volume **1,** pp. 284–306. Prentice-Hall, Inc., Englewood Cliffs, NJ.

Gastil, R. G. (1968) Fault systems in northern Baja California and their relation to the origin of the Gulf of California. In *Proceedings of Conference on Geologic Problems of the San Andreas Fault System*, pp. 283–286. Stanford University Publications in Geological Sciences, Palo Alto, California, **11**.

Gastil, R. G. and Krummenacher, D. (1977) Reconnaissance geology of coastal Sonora between Puerto Lobos and Bahía Kino. *Geological Society of America Bulletin* **88,** 189–198.

Gastil, R. G., Phillips, R. P. and Allison, E. C. (1975) Reconnaissance geology of the state of Baja California. *Geological Society of America Memoir*, **140**.

Gephart, J. W. (1990a) FMSI: A FORTRAN program for inverting fault/slickenside and earthquake focal mechanism data to obtain the regional stress tensor. *Computers and Geosciences* **16,** 953–989.

Gephart, J. W. (1990b) Stress and the direction of slip on fault planes. *Tectonics* **9,** 845–858.

Gephart, J. W. and Forsyth, D. W. (1984) An improved method for determining the regional stress tensor using earthquake focal mechanism data: Application to the San Fernando earthquake sequence. *Journal of Geophysical Research* **89,** 9305–9320.

Goddard, E. N. *et al.* (1965) *Geologic map of North America*. United States Geological Survey.

Goff, J. A., Bergman, E. A. and Solomon, S. C. (1987) Earthquake source mechanisms and transform fault tectonics in the Gulf of California. *Journal of Geophysical Research* **92,** 10,485–10,510.

Grover, T. M., Heath, R., Walls, C., Miller, M. M. and Rubin, C. M. (1993) Evidence for active faulting in Valle de San Felipe, northern Baja California, Mexico: Space-based observations of the transition from an oceanic to continental transform boundary. *Geological Society of America Abstracts with Programs* **25,** A–481.

Hamilton, W. (1971) Recognition on space photographs of structural elements of Baja California. *United States Geological Survey Professional Paper* **718**.

Hausback, B. P. (1984) Cenozoic volcanic and tectonic evolution of Baja California Sur, Mexico. In *Geology of the Baja California Peninsula*, eds V. A. Frizzell, pp. 219–236. Society of Economic Paleontologists and Mineralogists, Pacific Station, Los Angeles, **39**.

Henry, C. D. (1989) Late Cenozoic Basin and Range structure in western Mexico adjacent to the Gulf of California. *Geological Society of America Bulletin* **101,** 1147–1156.

Humphreys, E. D. and Weldon, R. J. II (1991) Kinematic constraints on the rifting of Baja California. In *The Gulf and Peninsular Province of the Californias*, eds J. P. Dauphin and B. R. T. Simoneit, pp. 217–229. American Association of Petroleum Geologists Memoir, **47**.

Karig, D. E. and Jensky, W. (1972) The protogulf of California. *Earth and Planetary Sciences Letters* **17,** 169–174.

Larson, R. L., Menard, H. W. and Smith, S. M. (1968) Gulf of California: A result of ocean-floor spreading and transform faulting. *Science* **161,** 781–784.

Lee, J., Miller, M. M., Crippen, R., Hacker, B. and Ledesma Vasquez, J. (1996) Middle Miocene extension in the Gulf Extensional Province, Baja California: Evidence from the southern Sierra Juarez. *Geological Society of America Bulletin* **108,** 505–525.

Legg, M., Wong, O. V. and Suarez V., F. (1991) Geologic structure and tectonics of the inner Continental Borderland of northern Baja California. In *The Gulf and Peninsular Provinces of the Californias*, ed J. P. Dauphin and B. R. T. Simoneit, pp. 145–177. American Association of Petroleum Geologists Memoir, **47**.

Lewis, C. J. (1994) Constraints on extension in the Gulf Extensional Province from the Sierra San Fermín, northeastern Baja California. Ph.D. thesis. Harvard University.

Lewis, C. J. (1996) Stratigraphy and geochronology of Miocene and Pliocene volcanic rocks in the Sierra San Fermín and southern Sierra San Felipe, Baja California, Mexico. *Geofísica Internacional* **35,** 3–25.

Lewis, C. J. and Stock, J. M. (in press) Paleomagnetic evidence of localized rotation during Neogene extension in the Sierra San Fermín, northeastern Baja California, Mexico. *Journal of Geophysical Research*.

Lonsdale, P. (1989) Geology and tectonic history of the Gulf of California. In *The eastern Pacific Ocean and Hawaii*, eds E. L. Winterer, D. M. Hussong and R. W. Decker, pp. 499–521. Geological Society of America, The Geology of North America.

Lyle, M. and Ness, G. E. (1991) The opening of the southern Gulf of California. In *Gulf and Peninsula Provinces of the Californias*, eds J. P. Dauphin and B. R. T. Simoneit, pp. 403–423. American Association of Petroleum Geologists Memoir, **47**.

Mammerickx, J. and Klitgord, K. D. (1982) Northern East Pacific Rise: Evolution from 25 m.y. B.P. to the Present. *Journal of Geophysical Research* **87,** 6751–6759.

Marrett, R. and Allmendinger, R. W. (1990) Kinematic analysis of fault-slip data. *Journal of Structural Geology* **12,** 973–986.

Moore, D. G. and Buffington, E. C. (1968) Transform faulting and growth of the Gulf of California since the late Pliocene. *Science*, **161,** 1238–1241.

Nagy, E. A. (1997) Extensional deformation and volcanism within the northern Puertecitos Volcanic Province, Sierra Santa Isabel, Baja California, Mexico. Ph.D. thesis. California Institute of Technology.

Ortlieb, L., Ruegg, J. C., Angelier, J., Colletta, B., Kasser, M. and Lesage, P. (1989) Geodetic and tectonic analysis along an active plate boundary: The central Gulf of California. *Tectonics* **8,** 429–441.

Parker, R. L. and McNutt, M. K. (1980) Statistics for the one-norm misfit measure. *Journal of Geophysical Research* **85,** 4429–4430.

Pollard, D. D., Saltzer, S. D. and Rubin, A. M. (1993) Stress inversion methods: are they based on faulty assumptions? *Journal of Structural Geology* **15,** 1045–1054.

Sawlan, M. C. and Smith, J. C. (1984) Petrologic characteristics, age and tectonic setting of Neogene volcanic rocks in Northern Baja California Sur. In *Geology of the Baja California Peninsula*, ed. V. A. Frizzell, pp. 237–251. Society of Economic Paleontologists and Mineralogists, Pacific Section, Los Angeles, **39**.

Scotti, O., Nur, A. and Estevez, R. (1991) Distributed deformation and block rotation in three dimensions. *Journal of Geophysical Research* **96,** 12,225–12,243.

Slyker, R. G. (1974) Geophysical survey and reconnaissance geology of the Valle de San Felipe area, Baja California, Mexico. In *Geology of Peninsular California*, pp. 107–120. Society of Economic Paleontologists and Mineralogists, Pacific Section, Los Angeles.

Spencer, J. E. and Normark, W. R. (1979) Tosco–Abreojos fault zone; A Neogene transform plate boundary within the Pacific margin of southern Baja California. *Geology* **7,** 554–557.

Stock, J. M. (1989) Sequence and geochronology of Miocene rocks adjacent to the Main Gulf Escarpment: Southern Valle Chico, Baja California Norte, Mexico. *Geofísica Internacional* **28-5,** 851–896.

Stock, J. M. (1993) *Geology of southern Valle Chico and adjacent regions, Baja California, Mexico*, MCH076. Geological Society of America Map and Chart Series.

Stock, J. M. and Hodges, K. V. (1989) Pre-Pliocene extension around the Gulf of California and the transfer of Baja California to the Pacific plate. *Tectonics* **8,** 99–115.

Stock, J. M. and Hodges, K. V. (1990) Miocene to Recent structural development of an extensional accommodation zone, northeastern Baja California, Mexico. *Journal of Structural Geology* **12,** 315–328.

Stock, J. M., Lewis, C. J. and Nagy, E. A. (1997) The Tuff of San Felipe: An extensive middle Miocene pyroclastic flow deposit in NE Baja California, Mexico. IAVCEI General Assembly, Puerto Vallarta, Mexico, **16**.

Stock, J. M., Martín-B., A., Suarez-V., F. and Miller, M. M. (1991) Miocene to Holocene extensional tectonics and volcanic stratigraphy of NE Baja California, Mexico. In *Geological Excursions in Southern California and Mexico*, eds M. J. Walawender and B. B. Hanan, pp. 44–67. Geological Society of America Guidebook, San Diego, California.

Stock, J. M., Martín-Barajas, A. and Tellez-Duarte, M. (1996) Early rift sedimentation and structure along the NE margin of Baja California. In *Field Conference Guide 1996*, eds P. L. Abbott and J. D. Cooper, pp. 337–372. Society of Economic Paleontologists and Mineralogists, Pacific Section, **80**.

Teyssier, C., Tikoff, B. and Markley, M. (1995) Oblique plate motion and continental tectonics. *Geology* **23,** 447–450.

Tron, V. and Brun, J. P. (1991) Experiments on oblique rifting in brittle–ductile systems. *Tectonophysics* **188,** 71–84.

Umhoefer, P. J., Dorsey, R. J. and Renne, P. (1994) Tectonics of the Pliocene Loreto basin, Baja California Sur, Mexico, and evolution of the Gulf of California. *Geology* **22,** 649–652.

Umhoefer, P. J. and Stone, K. A. (1996) Description and kinematics of the SE Loreto basin fault array, Baja California Sur, Mexico: a positive field test of oblique-rift models. *Journal of Structural Geology* **18,** 594–614.

Withjack, M. O. and Jamison, W. R. (1986) Deformation produced by oblique rifting. *Tectonophysics* **126,** 99–124.

Zanchi, A. (1994) The opening of the Gulf of California near Loreto, Baja California, Mexico: From Basin and Range extension to transtensional tectonics. *Journal of Structural Geology* **16,** 1619–1639.

APPENDIX 1A

Results For Best-fitting Model [No Known Pliocene/Quaternary Faults] (1)

Datum #	Observed Fault Plane			Slip Direction				
	Misfit of Fault Plane	Azimuth	Dip (2)	Trend	Plunge	Rake	Sense of Slip (3)	Low Shear Stress (4)
1	16	46	78	222	18	162	L	
2	18	334	86	334	7	7	L	*
3	24	99	73	126	56	60	L	
4	33	224	56	19	32	140	L	
5	12	12	81	102	81	90	N	
6	24	15	86	178	76	103	R	*
7	32	203	64	324	60	105	L	
8	24	252	62	69	6	173	L	
9	28	57	79	231	30	149	R	*
10	39	195	56	302	55	100	L	
11	21	286	17	286	0	0	L	
12	17	120	20	130	4	11	R	*
13	1	199	50	289	50	90	N	
14	3	60	90	60	25	25	L	
15	16	244	74	28	64	111	L	
16	5	251	79	341	79	90	N	
17	3	225	83	225	0	2	L	
18	2	225	83	228	25	25	L	
19	11	251	82	254	20	20	R	*
20	43	45	70	50	14	15	R	*
21	19	223	56	273	49	65	L	
22	5	88	90	268	90	90	N	
23	33	162	58	206	48	61	R	
24	22	72	74	206	68	104	L	
25	14	72	84	79	50	50	R	
26	20	57	74	57	0	0	L	
27	24	237	80	57	0	180	L	*
28	35	166	55	330	22	153	R	
29	39	230	60	50	0	180	R	*
30	3	222	27	307	27	86	L	
31	19	222	27	0	19	135	R	
32	23	80	72	80	0	0	L	
33	26	52	67	60	18	20	L	
34	6	220	70	310	70	90	N	
35	21	63	72	75	33	35	L	
36	27	60	78	237	15	165	R	*
37	1	237	82	248	54	55	L	
38	27	58	45	89	27	40	L	
39	4	201	53	299	53	95	N	
40	44	243	40	356	38	108	L	
41	16	244	74	27	65	110	L	
42	15	251	53	11	49	109	N	
43	21	352	65	32	54	63	N	
44	18	82	49	213	41	120	R	
45	45	30	51	162	43	120	L	
46	38	205	50	25	0	180	L	
47	3	259	88	260	25	25	L	
48	16	350	49	45	43	65	N	
49	4	270	88	87	60	120	N	
50	7	265	60	14	59	100	N	
51	2	260	87	260	0	0	L	
52	11	223	42	293	40	75	N	
53	26	230	60	230	0	0	L	
54	28	148	63	318	19	159	R	
55	4	215	83	215	0	2	L	
56	7	40	88	219	25	155	L	
57	22	41	71	221	0	180	L	
58	0	305	74	68	71	100	N	
59	7	32	40	97	37	70	N	
60	1	60	60	140	60	85	L	
61	0	80	56	170	56	90	N	
62	13	88	84	265	47	153	L	*
63	18	44	74	50	19	20	L	
64	35	215	55	9	32	140	L	
65	14	185	32	309	27	120	N	
66	2	227	85	46	10	170	L	
67	16	107	78	109	10	10	R	

68	6	15	44	105	44	90	N	
69	8	95	86	185	86	90	N	
70	9	126	84	306	0	180	R	
71	5	22	87	22	0	0	L	
72	9	180	88	357	60	120	N	*
73	7	265	60	14	59	100	N	
74	22	312	68	331	38	42	R	
75	29	348	56	122	47	118	R	
76	34	242	53	39	27	145	L	
77	14	208	70	325	68	100	R	
78	44	264	42	84	0	180	L	
79	9	30	60	84	54	70	N	
80	4	350	50	65	49	80	N	
81	14	220	70	236	37	40	L	
82	39	197	55	49	40	75	N	
83	4	312	10	345	5	32	N	
84	34	18	69	279	69	157	R	
85	9	35	66	215	24	90	N	*
86	14	73	80	163	90	2	L	
87	40	85	45	310	55	125	L	
88	13	217	74	127	90	180	L	
89	18	142	45	5	54	123	R	
90	26	345	64	103	46	51	R	
91	0	305	74	158	19	100	R	

(1) Principal stress axes (trend and plunge): $\sigma_1 = 351\ 85$, $\sigma_2 = 171\ 4$, $\sigma_3 = 81\ 0$; $\phi = 4.5$; $R = 0.9$; weighted average minimum rotation misfit, 17 degrees.
(2) Viewed in the azimuth direction, the fault dips to the right.
(3) Predominant fault motion; N, normal; L, left lateral; R, right lateral.
(4) Asterisk indicates that under best-fitting model this fault datum has low shear stress and is therefore not likely to have moved.

APPENDIX 1B

Results For Best-fitting Model [Pliocene/Quaternary Faults] (1)

	Observed Fault Plane			Slip Direction				
Datum #	Misfit of Fault Plane	Azimuth	Dip (2)	Trend	Plunge	Rake	Sense of Slip (3)	Low Shear Stress (4)
1	19	223	53	313	53	90	N	*
2	3	214	34	304	34	90	N	
3	31	44	78	214	39	140	L	*
4	16	265	80	85	0	180	R	
5	2	71	68	99	49	53	N	
6	19	192	52	252	48	70	N	
7	2	77	78	251	27	152	R	
8	8	79	54	259	0	180	L	*
9	15	243	65	243	0	3	L	
10	24	55	78	226	35	144	L	*
11	1	291	61	106	9	170	R	
12	12	279	81	99	0	180	R	
13	5	223	53	24	24	149	L	
14	30	225	64	355	58	110	N	*
15	24	55	78	226	35	144	L	*
16	29	88	84	265	28	152	L	*
17	4	45	90	225	10	170	L	
18	14	46	80	49	15	15	L	
19	6	78	54	236	28	146	L	
20	12	94	47	164	45	76	R	
21	3	27	76	27	0	0	L	
22	2	70	58	70	0	2	L	*
23	11	243	83	63	0	180	L	
24	1	62	90	62	75	75	L	
25	1	50	78	229	5	175	L	
26	1	11	73	11	0	0	L	
27	12	245	85	65	0	180	L	

(1) Principal stress axes (trend and plunge): $\sigma_1 = 341\ 30$, $\sigma_2 = 131\ 56$, $\sigma_3 = 243\ 14$; $\phi = -58.5$; $R = 0.1$; weighted average minimum rotation misfit, 11 degrees.
(2) Viewed in the azimuth direction, the fault dips to the right.
(3) Predominant fault motion; N, normal; L, left lateral; R, right lateral.
(4) Asterisk indicates that under best-fitting model this fault datum has low shear stress and is therefore not likely to have moved.